The Hong Kong Polytechnic University

Department of Health Technology and Informatics

Estimation of Young's Modulus and Poisson's Ratio of Soft Tissue using Indentation

Alex Pong Chi CHOI

A thesis submitted in partial fulfillment of the requirements for the degree of Master of Philosophy

AUG 2008

CERTIFICATE OF ORIGINALITY

I hereby declare that this thesis is my own work and that, to the best of my knowledge and belief, it reproduces no material previously published or written, nor material that has been accepted for the award of any other degree or diploma, except where due acknowledgement has been made in the text.

_____ **(Signed)**

CHOI Pong Chi, Alex **(Name of student)**

Abstract

Indentation is one of the widely used mechanical testing methods for biological soft tissue. Different from confined or unconfined compression test, *in-vivo* indentation test on soft tissues can be carried out in clinical application. However, to obtain Young's modulus of the tissue using indentation, its Poisson's ratio is traditionally assumed or obtained separately by another test which may cause experimental error and complexity. In this study, several calculation strategies were proposed to estimate Young's modulus and Poisson's ratio of soft tissue by single indentation simultaneously.

By finite element analysis, the effects of finite deformation on the double indentation method were studied. The results showed that the estimated Poisson's ratio and Young's modulus were larger than the actual values by up to 11.73% and 22.75%, respectively. Moreover, the feasibility of estimating Young's modulus and Poisson's ratio in single indentation with different deformations and deformation-dependent indentation stiffness was also verified separately. More accurate results could be obtained if the aspect ratio between indentor and tissue thickness was large enough. So, estimating Young's modulus and Poisson's ratio of soft tissue by single indentation might be more suitable to apply on thin soft tissue.

Beside finite element study, experiments on silicone phantoms were also carried out in this study. Mechanical indentations using material testing system and handheld tissue ultrasound palpation system were performed on two different kinds of silicone phantoms with the proposed calculation strategies. The comparison of the results between mechanical properties obtained by unconfined compression and proposed calculation algorithms revealed differently ranging from -3.1 % ~ 16.6 % in a harder

silicone phantom. The lager the aspect ratio was between the specimen thickness and indentor radius, the smaller the error was obtained.

After testing the feasibility of applying the proposed calculation strategies by the experiment on silicone phantoms, another experiment was performed on bovine patellar articular cartilage for estimating the Young's modulus and Poisson's ratio of Articular Cartilage. Four bovine patellae were tested before and after trypsin enzyme digestion using these two calculation strategies. The Poisson's ratio and Young's modulus of cartilage estimated by single indentation using deformation-dependent indentation stiffness ranged from 0.45 – 0.47 and 1.33 MPa – 2.21 MPa, respectively. While the Poisson's ratio and Young's modulus of cartilage estimated by single indentation with the information of different deformations ranged from 0.46 – 0.49 and 1.39 MPa – 2.40 MPa. The percentage changes of the results obtained using the two different proposed algorithms were less than 6 % for Poisson's ratio and 9 % for Young's modulus. The Young's modulus of cartilage after trypsin enzyme digestion was found to be greatly reduced by around 45 %.

The results revealed that the proposed algorithms could improve the accuracy of estimation of Young's modulus and also be useful for calculating shear modulus. Further studies should be conducted to develop new finite element models, using indentors with different radii and applying non-destructive techniques for thickness measurement. The effects of changes in tissue thickness in indentation on the estimation results should be further studied and a novel hand-held indentation technique may be developed in the future.

Keywords: Young's modulus; Poisson's ratio; Indentation; Finite element study; soft tissue; thickness measurement; stiffness measurement

Publications

Publications and Intellectual Properties directly related to this study

Year	Title
2006	Zheng, Y. P., Ling, H. Y. and Choi, A. P. C., Indentation technique for simultaneous estimation of Young's modulus and Poisson's ratio of soft tissues. Invited book chapter for "*International MRW on Biomechanics systems"*. Jun 2006.
2006	Zheng, Y. P. and Choi, A. P. C., Measurement of Young's modulus and Poisson's ratio simultaneously from indentation. US Provisional Patent Application. No. 60/580,679. Chinese patent filed. 200610077789. 6 Apr 2006.
2006	Zheng, Y. P., Choi, A. P. C., Ling, C. H. Y., Estimation of Poisson's ratio by using force and deformation information from single indentation. *5th International conference on the Ultrasonic Measurement and Imaging of Tissue Elasticity.* Oct 8-11 2006, Snowbird, Utah, US, p101.
2006	Choi, A. P. C., Zheng, Y. P., Ling, H. Y. and He, J. F., Estimation of mechanical properties of soft tissues using ultrasound indentation with deformation dependent characteristics. *Biomedical Engineering Conference, Hong Kong*, Sept 21-23, 2006. p4-6.
2006	Choi, A. P. C. and Zheng, Y. P., Estimation of Young's modulus and Poisson's ratio simultaneously using single indentation: A potential method for articular cartilage assessment. *6th Symposium of International Cartilage Repair Society*, Jan 8-11, 2006, San Diego, CA, US.
2005	Choi, A. P. C. and Zheng, Y. P., Estimation of Young's modulus and Poisson's ratio of soft tissue from indentation using two different-sized indentors: finite element analysis of the finite deformation effect. *Med. Biol. Eng. Comp.*, 43, 258-264, 2005.
2004	Choi, A. P. C. and Zheng, Y. P., The effects of deformation on the Young's modulus measurement by two sized indentors – finite element simulation study. *3rd International Conference on the Ultrasonic Measurement and Imaging of Tissue Elasticity*, Oct 17-20 2004, Cumbria, UK, p24.

Other publications with my contributions during the study period

Year	Title
2007	Huang, Y. P., Zheng, Y. P., Leung, S. F. and Choi, P. C., High frequency ultrasound assessment of skin fibrosis: Clinical results. *Ultrasound in Med. & Biol*. 33(8), 1191-1198, 2007b.
2007	Ling, H. Y., Choi, P. C., Zheng, Y. P. and Lau, K. T., Extraction of mechanical properties of foot plantar tissues using ultrasound indentation associated with genetic algorithm, *J. Mat. Science–material in Med.* 18(8), 1579-1586, 2007.
2007	Ling, H. Y., Choi, P. C., Zheng, Y. P. and Lau, K. T., Study on the mechanical properties of tissue-mimicking phantom composites using ultrasound indentation. Key *Eng. Mat.* 334-335, 133-136, 2007.
2006	Zheng, Y. P., Li, Z. M., Choi, A. P. C., Lu, M. H., Chen, X. and Huang, Q. H., Ultrasound palpation sensor for tissue thickness and elasticity measurement – Assessment of transverse carpal ligament. *Ultrasonic*, 44, E313-E317, Suppl 1, 2006.
2006	Ling, H. Y., Choi, P. C., Zheng, Y. P. and Lau, K. T., Study on the mechanical properties of tissue-mimicking phantom composites using ultrasound indentation. *5th Asia-Australasian Conference on Composite Materials (ACCM-5)*. Nov 27-30 2006, Hong Kong. Paper ID 189-H
2006	Li, Z. M., Zheng, Y. P., Lu, M. H., Choi, A. P. C. and Huang, Q. H., Ultrasonic palpation of carpal tunnel mechanics, *52nd Annual Meeting of the Orthopaedic Research Society*, Mar 19-22, 2006, Chicago, IL, US.
2005	Zheng, Y. P., Chen, X. and Choi, P. C., Ultrasound Palpation Sensor for Tissue Thickness, Elasticity and Viscoelasticity. *World Congress on Ultrasonics merged with Ultrasonics International, WCU/UI'05*, Aug 28 – Sept 1, 2005-03-23, Beijing, China. p24.
2005	Zheng, Y. P., Choi, A. P. C. and Chen, X., Tissue Ultrasound Palpation System (TUPS) for Quantitative and Objective Soft Tissue Assessment. *Symposium on Advanced Technology for Health Care and Hygiene Control*, 27th May 2005, Hong Kong SAR. MD3.2.
2004	Choi, P. C., Zheng, Y. P., Wan, J., Ng, K. H. and Wong, K., Assessment of Stiffness and Thickness of Plantar Tissues of Diabetic Feet using Ultrasound. *11th World Congress of the International Society for Prosthetics & Orthotics*, Aug 1-6, 2004, Hong Kong. P335.

Acknowledgement

I am glad to take this opportunity to acknowledge all the people who have helped me during the last four years when I first worked as a research assistant and then had my postgraduate study at The Hong Kong Polytechnic University. Without their kind help, I could not have started and finished my research works.

Firstly, I would like to express my respects and hearty thanks to my supervisor, Prof. Yongping ZHENG, for his invaluable comments, guidance and encouragement throughout my study. Prof. ZHENG gave me a lot of opportunities to present my research works, publish academic articles and take part in different research projects. He is always full of enthusiasm and energy in research and development together with teaching the subject of biomedical engineering, which sets a model for me. His attitude and encouragement have affected and motivated me no matter in doing research or working in other fields of biomedical engineering.

I would like to express my deep thanks to Dr. Carrie LING for her great supports and helps in my experiments and thesis preparation. Dr. LING gave me a lot of advises and helps in the mechanics and material sciences.

I would also like to thank all the staffs in the Jockey Club Rehabilitation Engineering Centre and the Department of Health Technology and Informatics for

providing me the helps and necessary supports for my study.

My sincere thanks are also given to my colleagues in Bioinstrumentation Laboratory, Biomaterial & Biomechanical Testing Laboratory and Biomechanics Laboratory, including Dr. Xin CHEN for his kind help in Matlab program and Tissue Ultrasound Palpation System; Dr. Tracy LU for her generous help in finite element analysis, phantom preparation and advises in biomechanics of indentation; Dr. Qing Hua HUANG for his supports in the user program of TUPS; Dr. Qing WANG for her supports in experimental setup and advises in trypsin digestion; Mr. Sushil PATIL for his advises in patella specimen preparation; Prof. Ming ZHANG, Dr. Jason CHEUNG and Dr. Wilson LEE for their valuable helps and advises in the finite element analysis. Besides, I would like to thank other colleagues, including Mr. Yan Ping HUANG, Ms. Cris LIU, Dr. Anthony SUM, Ms. Grace LO, Dr. Jun Feng HE and Mr. James CHEUNG. They gave me a lot of encouragement and assistance in my project. Besides, I would also like to thank Ms. Sally Ding for her help in editing my thesis.

I would also like to thank my family, friends and brothers and sisters in my church for their supports and encouragement.

Finally, I would like to acknowledge the financial support from the Research Grant Council and the Hong Kong Polytechnic University for my research study and project.

Table of Contents

List of Figures

List of Tables

Abbreviations

a	Radius of indentor (unit: mm)
a/h	Area aspect ratio (radius/ original tissue thickness)
ADLs	Activities of Daily Living
ANOVA	Analysis of variance between groups
ArtC	Articular cartilage
β	Nonlinear factor depending on aspect ratio and Poisson's ratio
DOF	Degree of freedom
E	Young's modulus (unit: MPa, kPa)
ECM	Extra-cellular matrix
FE	Finite element
FEA	Finite element analysis
G	Shear modulus (unit: MPa)
GAG	Glycosaminoglycan
h	Original thickness (unit: mm)
H_A	Aggregate modulus
κ	Scaling factor depending on thickness and Poisson's ratio
κ_n	Scaling factor depending on thickness, Poisson's ratio and deformation
LVDT	Linear variable differential transformer
MRI	Magnetic resonance imaging
MTM	Material testing machine
NSAID	Non-steroidal anti-inflammatory drug
OA	Osteoarthritis
P	Indentation force (unit: N)

PBS	Phosphate buffered saline
PGs	Proteoglycans
PVC	Polyvinyl chloride
QLV	Quasi linear viscoelastic
RMS	Root mean square
SD	Standard deviation
SEM	Scanning electronic microscopy
SOS	Speed of sound
TUPS	Tissue ultrasound palpation system
US	Ultrasound
v	Poisson's ratio
w	Deformation (unit: mm)
w/h	Deformation ratio (deformation/ original tissue thickness)
X-ray	Radiography

Chapter 1 Introduction

Testing the mechanical properties of soft tissue was a common interest of healthcare professionals, because the changes of the tissue properties may be due to the physiological or pathological reasons. Therefore, the changes in mechanical properties of biological soft tissue could be an important clinical indicator for various diseases. In this chapter, the characteristics of soft tissues and different mechanical property testing methods are first reviewed. Various indentation models and the parameters for estimating the mechanical properties using indentation are also introduced.

1.1 Characteristics of Different Soft Tissues

According to National Cancer Institute of the United States, soft tissue refers to muscle, fat, fibrous tissue, blood vessel, or other supporting tissues of the body. In this section, three types of soft tissues, including articular cartilage, skin and muscle with associated connective tissues, were introduced to give a better understanding on the structure, composition and functions of soft tissue. Such information is crucial for the estimation of mechanical properties of soft tissue.

1.1.1 Articular Cartilage

Articular cartilage (ArtC), which is a white thin connective layer covering the articulating surfaces of the bones in the synovial joint, is mainly for reducing the frictions and wears between two bones during movement by its low friction coefficient (Mansour, J. M., 2004; Mow *et al*., 1974). As shown in figure 1, it shows that the cross section of ArtC layer can be divided into four zones (Mow *et al*., 1974). The superficial zone is the thinnest layer in ArtC (10~20% of total thickness) but contains the highest content of water (75~80%) and collagens (85% dry weight) (Mow *et al*., 2005). The second layer is the middle zone, which is the thickest layer in the whole ArtC (40~60% of total thickness) (Mow *et al*., 2005). The water and collagen contents decrease with increasing depth. The collagen fibers in middle zone are lesser than those in superficial zone which are loosely packed with random orientation (Buckwalter *et al*., 1991). The deep zone contributes nearly 30% of the total thickness of ArtC with the highest Proteoglycans (PGs) content and the lowest water content. Below the deep zone, the calcified zone is the interface layer between the deep zone and the subchondral bone plate. In this zone, the bundles of collagen fibers from the deep zone are inserted into the subchondral bone plate in order to provide a strong anchoring system for the tissue (Bullough and Jagannath, 1983).

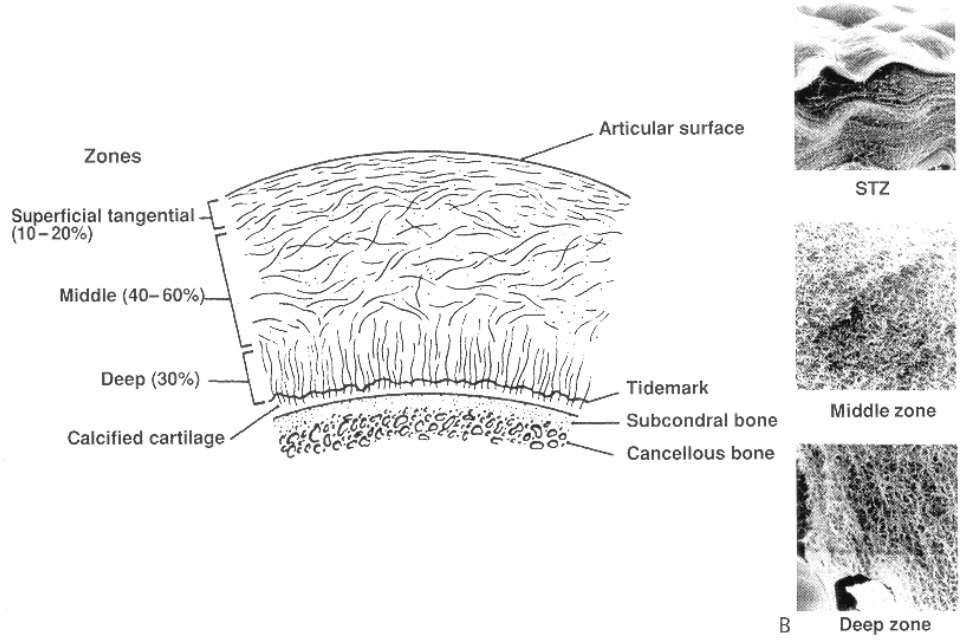

Figure 1 The schematic diagram and scanning electronic microscopy (SEM) (right hand sides) picture of ArtC (Mow *et al*., 1974)

As mentioned before, ArtC can be separated into four zones. It has been found that the orientations of the collagen fibers are different in each zone. So, the structural properties of the ArtC are heterogeneous and anisotropic. That is to say, the biomechanical properties of ArtC not only time-dependent due to different water composition in each layer, but also vary from different directions due to different orientations of collagen fibers (Wang *et al*., 2001; 2003; Chahine *et al*., 2004).

As mentioned before, water is one of the main compositions in the extra cellular matrix (ECM), the time dependent permeability of water content in the ArtC contributes to its viscoelasticity. The mechanical properties of ArtC depend on the

fluid flow in ECM (Hayes and Mockros, 1971; Parsons and Black, 1977). The variations of its mechanical properties are quite obvious in different kinds of species (Athanasiou *et al*., 1991) and various geometries (Jurvelin *et al*., 2000), which makes the mechanical properties ArtC unique and complicated.

As the function of ArtC is to distribute the force evenly on the bone surface and to reduce the friction at that interface, ArtC is mainly under compressive and shear forces in our daily activities. Osmotic swelling pressure (0.05 ~ 0.35 MPa) and collagen-PG solid matrix (0.5 ~ 1.5 MPa) (Armstrong and Mow, 1982) contribute to the compressive modulus of ArtC. ArtC is also under the shear force during the joint motion. The shear stiffness of ArtC is mainly contributed by the collagen-PGs interaction (Mow and Ratcliffe, 1997), which depends on the content of collagens.

1.1.2 Skin

Skin is the outermost layer of our human body, which can be simply divided into epidermis and dermis (Figure 2). The function of skin is protecting the internal organs, sensing the stimulation from the environment and regulating the body temperature. The composition of skin is relatively more complicated than that of ArtC. The layer of epidermis mainly consists of keratinocytes and to a lesser extent, melanocytes, Langerhans cells, Merkel cells and unmyelinated axons. The collagen fibers of the

epidermis are randomly oriented. The dermis layer consists of eccrine glands, apocrine glands, hair follicles, veins nerves, a fine network of collagen fibers, and the elastic fibers together with other components of the ECM (Oilarinen and Knuutinen, 2002). The structure of dermis is more irregular compared with that of epidermis. Collagen fibers play an important role not only in ArtC, but also in skin. Comparing with ArtC, there are different types of collagen in skin. Collagens contribute 72 % of the total dry weight in the dermal tissue, whereas Elastin and other ground substances contribute 4 % and 24 %, respectively (Uitto, *et al*., 1989).

The main function of the skin is to provide the physical barrier between the internal body and the environment. It not only plays an important role in the regulations of body temperature and water content, but acts as a shield to keep the antigens away from body. The mechanical properties of the skin are not similar to those of the ArtC. As the composition and structure of skin are more complicated compared with ArtC, skin is considered as a kind of highly inhomogeneous, anisotropic, viscoelastic and non-linear tissue.

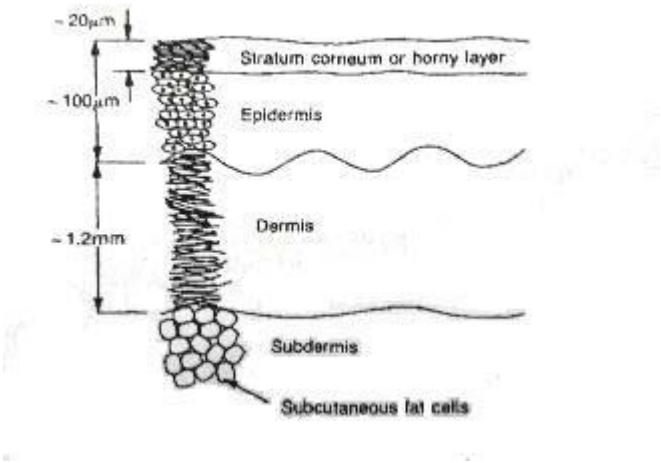

Figure 2 The schematic diagram of the skin with the information of thickness and orientation of the collagen fibers (Mow *et al*., 2005).

1.1.3 Muscle and Connective Tissues

Generally, there are three types of muscle, including cardiac, smooth and skeletal muscles. In this section, the skeletal muscle is discussed and reviewed, which is voluntarily controlled and striated in structure. It contributes to 40 - 45 % of the body weight. It is mainly responsible for the locomotion and maintenance of body posture (Tobias and Campello; 2001). Compared with other connective tissues, muscle is composed by two special fibers which are myosin (thick) and actin (thin) filaments (Figure 3).

Muscle contraction is achieved by the connection of cross-bridge of myosin filament to the troponin of actin filament and the pulling action toward each others. Both myosin and actin filament are the contractile part of myofibrils (Tobias and

Campello; 2001). For connective tissues, tendon is a typical example of the fiber type. However, the major component of the tendon is collagen and elastin (Nordin *et al*., 2001). The combination of tendons and muscles can be simply represented by a viscoelastic model, which is a combination of the Kelvin-Voigt and Maxwell bodies (Nordin *et al*., 2001).

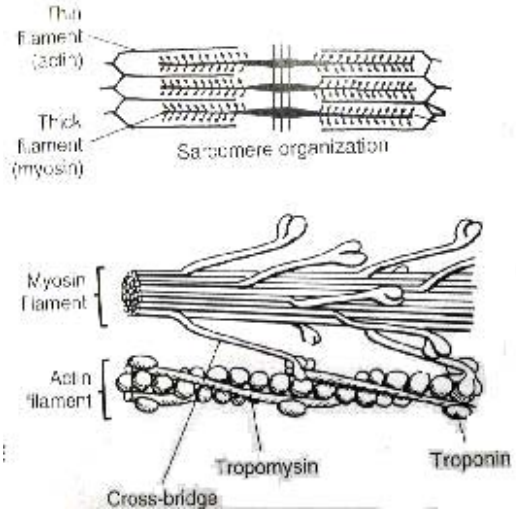

Figure 3 The schematic diagram of the actin and myosin filaments of the muscles, the cross bridge connects to troponin and pulls the different in series actin toward each other (Nordin *et al*., 2001).

1.2 Methods of Soft Tissue Mechanical Testing

As the structure and mechanical properties are quite different in various soft tissues, several testing methods have been developed by researchers to investigate them. In this section, compression, shear test, tensile test and indentation are briefly reviewed with the main focus on the indentation test.

1.2.1 Compressive Testing

Compression test is a common mechanical testing method for engineering materials. By measuring the compressive force and the corresponding material deformation, Young's modulus, which is the measure of the stiffness of the material, can be calculated by stress/ strain as follow:

$$E = \frac{F}{A} \Big/ \frac{w}{h} \tag{1}$$

where F is the compression force, A is the contact area, w is the deformation and h is the original thickness. The size of compressor is not less than the size of the material sample under the test. When the uniaxial compression force is applied to the tissue via the compressor, the material starts to deform and undergo the lateral extension. The ratio of the axial deformation to lateral deformation is called Poisson's ratio which ranges from 0 to 0.5 representing different mechanical properties from being totally compressible to totally incompressible.

There are two types of compression in biphasic model (solid and liquid phases of biological tissue), which are unconfined and confined compressions (Mow *et al.*, 1980). In unconfined compression, the Young's modulus *(E*) of the solid and liquid

phases could be obtained in instantaneous compression by the equation (1). Afterward, the aggregate modulus (H_A) could be obtained by the confined compression with the permeability and Poisson's ratio which would be discussed in the section of biphasic model. As shown in Figure 4, no lateral extension of material is allowed during confined compression Figure 4(a), while lateral displacement of material is allowed in unconfined compression Figure 4(b).

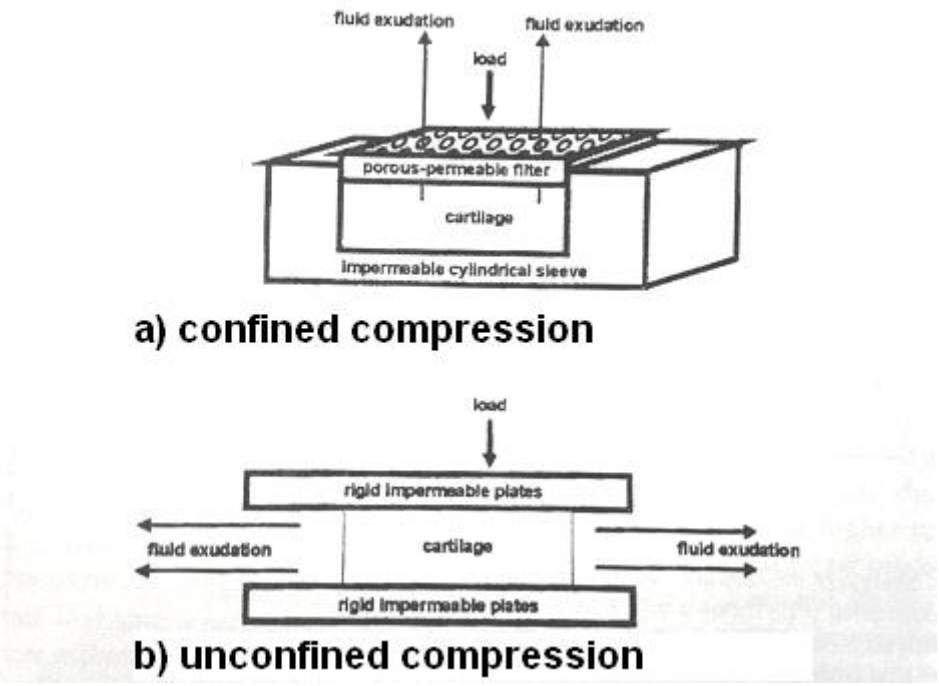

Figure 4 The schematic diagrams of confined compression (a) and unconfined compression (b) for biological tissue in biphasic model (Hasler *et al*., 1999).

Compression has been widely used for the testing of soft tissues. Confined and unconfined compression tests on pig skin were carried out for investigating the

viscoelastic properties of skin (Wu *et al*., 2003; 2007). Moreover, compression load was applied on the superficial muscle stiffness to study the pressure sores (Linder-Ganz and Gefen, 2004). The applications of compression test on ArtC have also been widely reported. Different mechanical properties of ArtC, such as depth dependent compression modulus (Schinagl *et al*., 1997), flow-independent viscoelasticity (Huang *et al*., 2001) and biphasic poroviscoelastic properties (DiSilvestro and Suh, 2001), have been studied.

1.2.2 Shear Testing

If the applied force to the material under test is in parallel with the material surface, that applied force is called shear force. Shear testing applies the shear force to the material and measures the corresponding deformation (Kristy *et al*., 1997). For a linear elastic material, the relationship between Young's modulus and Poisson's ratio is

$$\mu = \frac{\mathrm{E}}{2(1-\nu)} \tag{2}$$

where μ is shear modulus, E is the Young's modulus and ν is the Poisson's ratio.

The latest development is tri-axial shear testing on the biological soft tissue. By

using a highly precise device, tissue deformation due to the three directional compressive forces and three directional shear forces could be measured for calculating shear stiffness (Dokos *et al*., 2000). During the shear test, tangential force is exerting on the surface of the specimen. This test is suitable for testing ArtC compared with other kinds of soft tissues since a small piece of ArtC can be slit and put into a small device for the test (Setton *et al*., 1994).

1.2.3 Tensile Testing

Tensile test is another common method for testing engineering material, by providing pulling force on the material under test. Tensile modulus which is the ratio of the tensile stress to the deformation can be measured in this test. Tensile test is usually used for testing skin/ muscle or tendon (Lin *et al*., 1999). It can be applied to find not only the tensile modulus, but also the tensile strength by pulling the specimens until fracture.

1.2.4 Aspiration Testing

Aspiration test is another testing method to apply pulling force on the material under test. Nava *et al.* (2003) reported this method to determine the mechanical properties of human soft tissues. Different from the tensile test, a small sectional

cylindrical probe is applied on the material surface. A negative pressure is created inside the cylindrical probe for sucking the material under test into the circular probe with known radius. The deformation of the tissue can be captured by imaging device. The applied negative pressure and the tissue deformation can be used for calculate the tissue properties. This technique is useful for the measurement of human soft tissue, such as skin (Pedersen *et al.*, 2003), uterine cervices (Bauer *et al.*, 2007) and liver tissue (Mazza *et al.*, 2007).

1.2.5 Indentation Testing

With the similar experimental setup as compression, indentation is another common material testing method. The main difference between indentation and compression test is that the size of indentor surface is less than the testing surface of specimen. In general, the diameter of soft tissue should be at least 5 times more than that of indentor (Spilker *et al*., 1992). Compared with the compression, the main advantage of indentation is that *in-vivo* testing can be achieved non-invasively (Zheng and Mak, 1999; Suh *et al*., 2001; Toyras *et al*., 2001). There are two types of indentors including plane-ended cylindrical and spherical indentors. Different theoretical models have been developed for various shapes of indentor in the calculation of the tissue properties (Waters NE 1965a; 1965b; Hayes *et al*., 1972). Indentation has been

used for characterizing the mechanical properties of various soft tissues, including plantar foot (Zheng *et al*., 2000; Klasener *et al*., 2002), residual limb (Mak *et al*., 1994; Zheng and Mak, 1999a; 1999b), neck (Leung *et al*., 2004; Huang *et al*., 2005; 2007), breast (Han *et al*., 2003), buttock (Wang *et al*., 2000), skin (Lafrance *et al*., 1995; Dawes-Higgs *et al*., 2004; Lau *et al*., 2005), muscles (Zheng *et al*., 1999; Lasesner *et al*., 2001; 2002) and ArtC (Mow *et al*., 1989; Jurvelin *et al*., 1990; Athanasiou *et al*., 1991; Suh *et al*., 2001). Aiming to develop an *in-vivo*, non-invasive tissue testing technique for clinical use, indentation is the main focus of this study.

1.3 Indentation Models for Soft Tissues

1.3.1 Indentation Models

Many models for soft tissue indentation have been proposed by previous researchers, including single phasic model (Hayes *et al*., 1972), biphasic model (Mak *et al*., 1987; Mow *et al*., 1989), triphasic model (Lai *et al*., 1991) and other different models, as introduced in the following subsections.

1.3.1.1 Single Phasic Model

In 1972, Hayes *et al*. proposed a rigorous mathematical solution for indentation of ArtC using a flat-ended cylindrical indentor (Figure 5), the Young's modulus (E)

can be expressed as follows:

$$E = \frac{\left(1-v^2\right)}{2a\kappa\left(a/h, v\right)}\frac{P}{w} \tag{3}$$

where v is the Poisson's ratio, P is the indentation load, w is the indentation depth, a is the radius of indentor, h is the tissue thickness and κ is the scaling factor for geometry effects, which depends on Poisson's ratio and aspect ratio a/h (the ratio between indentor radius and original thickness of tissue). In their studies, ArtC was modeled as a homogenous, isotropic and linear elastic material. This equation is based on the assumptions of infinitesimal deformation and frictionless tissue-indentor interface. Hayes *et al.* (1972) provided a set of κ based on different v and a/h.

Young's modulus and shear modulus were used to describe mechanical properties of ArtC via the Hayes' equation, and the Poisson's ratio should be known in advance. In the single phasic model, indentation of ArtC can be simulated as instantaneous and equilibrium responses. Instantaneous response occurs with high indentation rate when tissue fluid does not have sufficient time to flow out from ECM. If the indentation rate is low enough, the tissue fluid could completely flow out and result in the equilibrium response. Pervious results showed that the indentation rate between 0.75 mm/s and 7.50 mm/s is still valid for using Hayes' model (Zheng *et al*.,

1999). This model has been applied to the studies on various soft tissues, including skin with tissue fibrosis, burn scar, diabetic foot, muscles, residual limb (Zheng and Mak, 1999a; 1999b; Zheng *et al*., 1999; 2000; Leung *et al*., 2002; Lau *et al*., 2005; Huang *et al*., 2005; 2007a; 2007b).

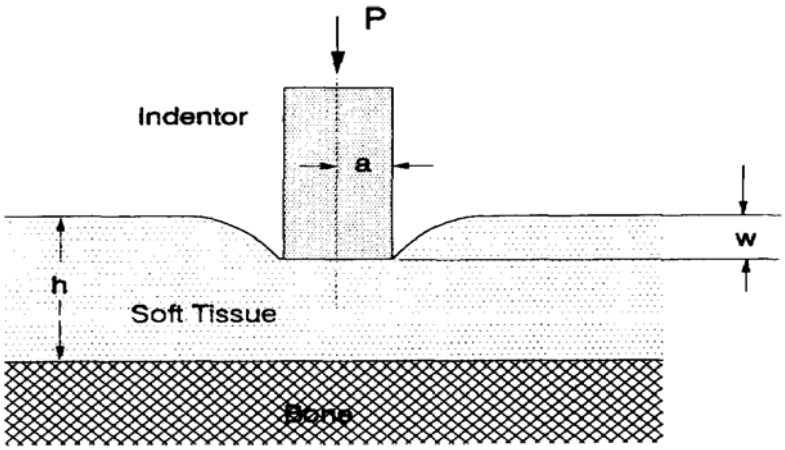

Figure 5 The schematic diagram of the single phase model indentation with a plane-ended indentor (Hayes *et al*., 1976).

Frictionless tissue-indentor interface is one of the prerequisite of Hayes' equation. Zhang *et al*. (1997) reported that the effects of friction at tissue-indentor interface became more significant when the Poisson's ratio was close to 0.5. If the aspect ratio a/h was small enough, the effects of friction could be minimized (Zhang *et al*., 1997). It is because the material cannot be compressed during the indentation, the expansion of soft tissue generate the shear force and act on the indentor interface.

Another prerequisite is infinitesimal deformation, but it cannot be achieved in practice by manual indentation. Therefore, Zhang *et al*. (1997) included the finite deformation effects in the equation (3) as

$$E = \frac{\left(1-v^2\right)}{2a\kappa\left(a/h, v, w/h\right)}\frac{P}{w} \tag{4}$$

In comparison with equation (3), the scaling factor κ in equation (4) depends not only on aspect ratio a/h and Poisson's ratio v, but also deformation ratio w/h. In this study, an axisymmetric solid 4-node bilinear elements (CAX4) finite element (FE) model was built for estimating various kappa values in the situation with different aspect ratios, Poisson's ratios and deformation ratios.

1.3.1.2 Viscoelastic and Quasi-Linear Viscoelastic Models

It is well known that biological soft tissue is viscoelastic. Some studies was applied the Kelvin – Voigt model which is a combination of the springs and dashpots for the demonstration of viscoelastic behaviors of soft tissues. The linear springs represent the elasticity of instantaneous proportion between stress and strain, whereas the dashpots represent the viscosity that is the proportion of stress to velocity (Hayes and Mockros, 1971; Parsons and Black, 1977). During indentation, the parameters of

force, deformation and time are used to estimate the viscoelastic properties of soft tissues associated with various mathematical algorithms.

Fung (1972) proposed the quasi-linear viscoelastic (QLV) model to describe the force-deformation relationship of soft tissue, the load response $\mathrm{T}(t)$ can be expressed as

$$\mathrm{T}(t) = \int_{-\infty}^{t} G(t-\xi) \cdot \frac{\partial \mathrm{T}^{e}(\mu(\xi))}{\partial \mu(\xi)} \cdot \frac{\partial \mu(\xi)}{\partial \xi} \cdot d\xi \tag{5}$$

where, T*(t)* is the stress at any time (t), $\mu(t)$ was expressed in terms of a convolution integral of a reduced relaxation function $G(t)$ and $\mathrm{T}^{e}(\mu)$ is nonlinear elastic function (Fung, 1972; 1981). By implementing the QLV model into the linear elastic indentation solution (Zheng and Mak, 1999), the indentation load $P(i)$ can be expressed as

$$P(i) = \frac{2ah}{1-\nu^{2}} \left[\kappa(h,u(i)) \left[E_{0}u(i) + E_{1}u^{2}(i) \right] - \frac{\alpha}{\tau} \sum_{j=1}^{i} \kappa(h,u(i-j)) \left[E_{0}u(i-j) + E_{1}u^{2}(i-j) \right] e^{-j \cdot dt/\tau} dt \right] \tag{6}$$

where dt is the time interval between two continuous data points, is the basic imaginary unit which represents a moment of infinitesimal indentation, *a* is the

indentor radius, *h* is the tissue thickness, *v* is the Poisson's ratio. Similar to equation (4), κ is the scaling factor for geometry effects, which depends on aspect ratio, Poisson's ratio and deformation ratio. Using equation (6), $P(i)$ can be predicted from the indentation response $u(i)$ and the four material parameters including initial modulus E_0, nonlinear factor E_1, time constant τ, and viscosity-related constant α. Therefore, the viscoelastic properties can be estimated by optimizing different computational methods via minimizing the root mean squared (RMS) error between equation (6) and the load-deformation data.

1.3.1.3 Biphasic Model

In the single phasic model, soft tissue is considered as a single homogenous medium. On the other hand, the viscoelastic properties are partly attributed to the interstitial fluid flows in and out of the ECM of soft tissue (Mak *et al*., 1987). In 1980, linear biphasic theory was proposed to model the ArtC as a soft tissue with solid and liquid phases (Mow *et al*., 1980). Both phases in linear biphasic model were assumed to be incompressible and immiscible. The solid phase was assumed to be porous, homogenous, isotropic, permeable, and linear elastic. For the liquid phase, it was assumed to be nonviscous. The total stress σ^T acting on the ArtC is the summation of the stress acting on solid phase σ^S and the stress acting on fluid phase σ^F, as

the following equation:

$$\sigma^T = \sigma^S + \sigma^F . \tag{7}$$

Afterwards, Mak *et al*. and Mow *et al*. developed a linear biphasic indention method for the theoretical and experimental analyses of ArtC (Mak *et al*., 1987; Mow *et al*., 1989). The theoretical indentation creep solution depends on the similarity variable $t' = t/\left(a^2/kH_A\right)$, where a is the radius of indentor, k is the scaling factor and H_A is the aggregate modulus. Besides, theoretical indentation creep depends on other three dimensionless parameters including 1) the indenting load $P_o/\left(2\mu_s a^2\right)$, 2) the aspect ratio a/h and 3) the Poisson's ratio of the solid phase v_s. The solution of the indentation creep μ can be written as

$$\mu\left[\log_{10}(t), S\right]/h = G\left[\log_{10}(t); S, P_o/\left(2\mu_s a^2\right), a/h, v_s\right]. \tag{8}$$

In the above equation (8), the aspect ratio a/h is known, indenting load $P_o/\left(2\mu_s a^2\right)$ and creep displacement μ can be measured, so, this equation actually shows the relationship between the Poisson's ratio and time. For any specific time, there is a corresponding creep response. When $t' \rightarrow \infty$, the $S \rightarrow 0$ and the creep results become

$$\frac{\mu(\infty)}{h} = \frac{a}{h}\left[\frac{P_o}{2a^2\mu_s}\right]\left[\frac{\left(1-v^2\right)}{2\kappa\left(a/h, v_s\right)}\right] \tag{9}$$

where $\mu(\infty)$ is the creep displacement when $t' \rightarrow \infty$, μ_s is the shear modulus of the solid matrix, *h* is the original thickness, *a* is the radius of the indentor, *Po* is the load used in the indentation, kappa (κ) is the scaling factor, which has been determined in pervious studies (Hayes *et al*., 1972; Jurvelin J., 1991). By using equation (9), the various master solutions were calculated in terms of different *u*/*h* and *t.* In comparison with the corresponding master solution curve, the experimental curve can be obtained by getting the *u*/*h* against *t* curve.

Figure 6 shows an example of comparison between experimental *u*/*h* against t curve with master solution curves (Mow *et al*., 1989). In the equilibrium response, the Poisson's ratio is 0.5 (Kempson *et al*., 1971), equation (8) can be written to express shear modulus μ_s as follows:

$$\mu_s = \frac{P_o}{8a\left(u_o\right)\kappa\left(a/h, 0.5\right)} \tag{10}$$

where u_o is the instantaneous displacement of the indentor (Mak *et al*., 1987). After

calculate the Poisson's ratio v_s and shear modulus μ_s, The Young's modulus also can be calculated by the following equation:

$$E = 2\mu(1+v) \tag{11}$$

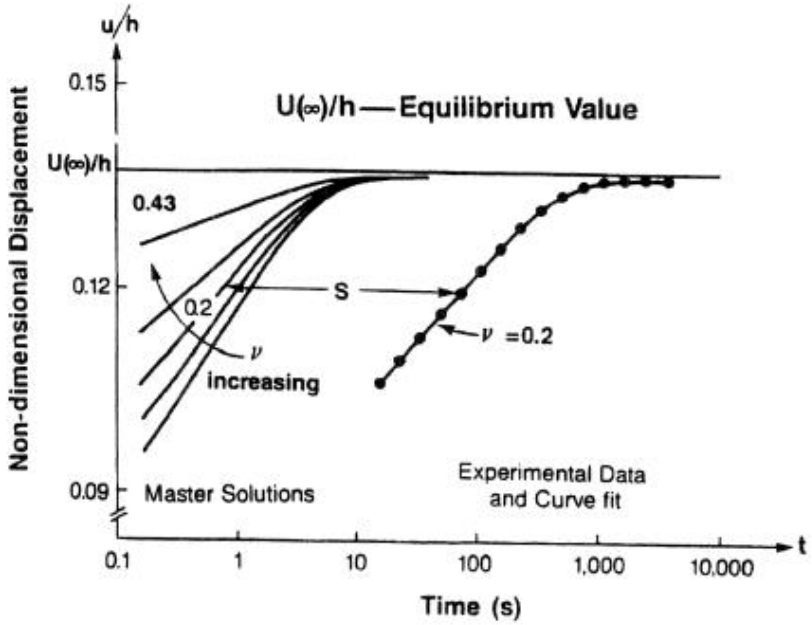

Figure 6 The graph shows the μ/h against t curves with different Poisson's ratio, which can be obtained by comparing the time shift factor (*S*) between experimental curve (right hand side) and master solution (left hand side) (Mow *et al.*, 1989).

Besides, aggregate modulus (H_A) can be obtained from Poisson's ratio (Figure 7) and shear modulus by the following equation:

$$H_A = \frac{2\mu(1-v)}{1-2v}. \tag{12}$$

Moreover, time-dependent properties are directly related to the fluid flow of ECM, so permeability *k* of fluid is essential to describe the viscosity of soft tissue which can be expressed as follows:

$$k = \left(a^2 / H_A\right) 10^{-S} \tag{13}$$

where *S* is the time shift factor, which can be found by the graph between the master solution and the experimental curve, H_A is aggregate modulus which can be found by equation (12), *a* is the radius of the indentor (Mak *et al.*, 1987).

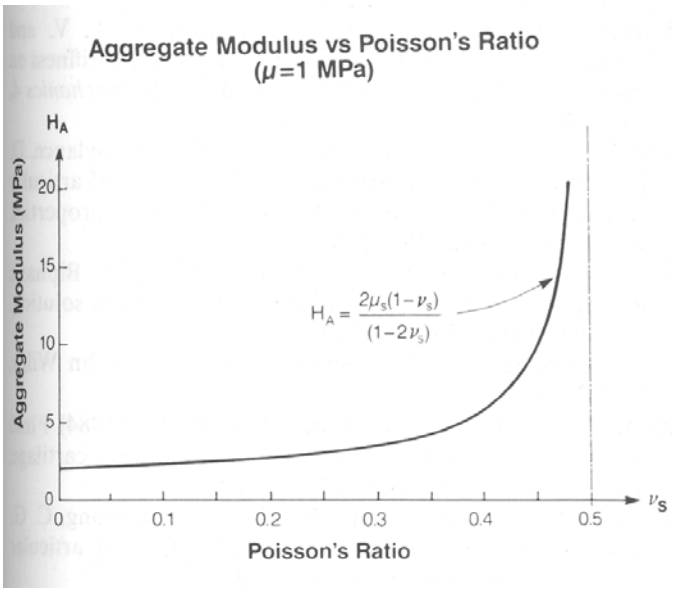

Figure 7 The relationship between aggregate modulus and Poisson's ratio when shear modulus is = 1 MPa using equation (12) (Mow *et al.*, 1989).

The apparatus used in the biphasic indentation is complicated (Figure 8). One of the major differences between biphasic indentation and single phasic indentation is in the indentor. The indentor used for biphasic indentation is porous. Therefore, the indentor is able to allow the fluid flow at indentor-tissue interface (Mow *et al*., 1989). Moreover, the indentation rate is applied to the biphasic model for calculating the permeability and Poisson’s ratio, so it is not easy to develop the hand-held biphasic indentation technique due to the difficulty to keep steady indentation rate in hand-held device for biphasic indention.

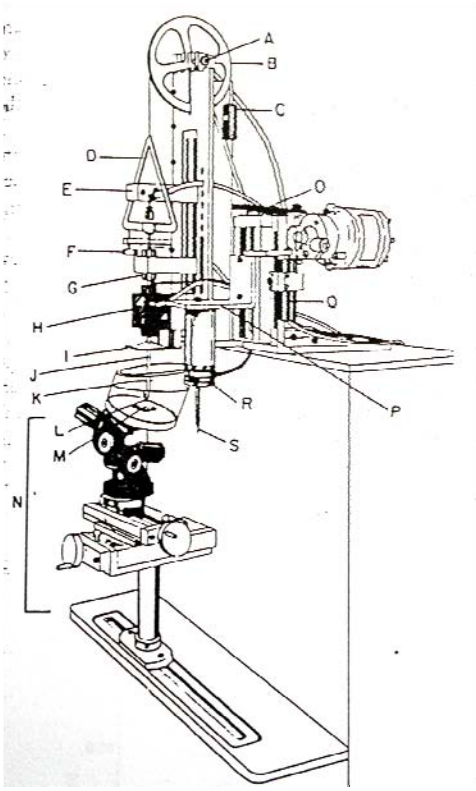

Figure 8 The experimental setup of the biphasic indentation used by Mow *et al*. in 1989, where S is the needle probe for needle punching measurement of cartilage thickness, N is the clamping system to adjust the orientation of the specimen for perpendicular indentation and J is the Porous indentor (Mow *et al*., 1989).

Following the linear biphasic indentation, nonlinear biphasic model including strain dependent permeability and flow-dependent properties was further studied (Lai *et al*., 1981). In Lai's study, the permeability was assumed to be constant. Mak *et al*. extended this idea to the biphasic proviscoelastic theory to address both the flow dependent and independent viscoelastic properties (Mak *et al.*, 1986).

1.3.2 Existing Techniques for Measurements of Soft Tissues

In order to estimate the mechanical properties of soft tissue, many parameters have to be obtained before the test. Single phasic indentation is the main focus in this study. The existing techniques for the measurement of thickness, deformation, force and Poisson's ratio are discussed in the following subsections.

1.3.2.1 Thickness and Deformation

Tissue thickness and deformation under indentation are the important parameters for the calculation of mechanical properties. Waters (1965) firstly considered the effects of thickness of tissue in the calculation of mechanical properties of soft tissue. Many modalities of thickness measurement have been employed in the previous studies of soft tissue, such as the linear variable differential transformer (LVDT), electromagnetic digitizer (Vannah *et al*., 1999), electromechanical digitizer (Klaesner *et al*., 2001; 2002), ultrasound (US) transducer (Zheng and Mak, 1996; Toyras *et al*., 2001) and magnetic resonant imaging (MRI) (Gefen *et al*., 2001; Nieminen *et al*., 2004).

All of the above mentioned methods can be used to determine the deformation during indentation. Every method has its advantages and disadvantages for specific

purposes. For example, LVDT is usually a part of material testing machine (MTM) with the results relatively reliable. However, due to the large size and setting of MTM, it is difficult to do *in-vivo* experiment using MTM. So, portable indentors with electromagnetic sensor, electromechanical sensor and US transducer were developed for more flexible in-vivo measurements. But, one of the drawbacks of using electromagnetic sensor is that it is easily interfered by other electrical driven devices. Moreover, the resolution of electromechanical sensor is not sufficient to detect the finite deformation of soft tissue. Furthermore, the US measurement of tissue deformation depends on the knowledge of sound speed in different types of soft tissue. Therefore, the results from the above three methods used in the handheld device may not be as accurate as using LVDT for measurement in MTM.

On the other hand, MRI can provide high resolution image for in-vivo study, however, it has difficulty in identifying boundaries of various soft tissues in the image for the calculation of deformation. Moreover, it is not cost-effective to apply the MRI method in the study with a large number of subjects. Compared with the measurement of deformation, the measurement of tissue thickness is relatively more difficult particularly when the measurement is performed in a minimally invasive way. In 1956, Garn reported that the tissue thickness measured by pinch-caliper is only equal to 65% of the original thickness of the tissues including skin and fat (Garn S, M., 1956).

Different methods have been used for measuring the thickness of various soft tissues. For ArtC, microscopic (Jurvelin *et al*., 1987; 1995), needle punching (Hoch *et al*., 1983; Swann and Seedhom, 1989; Mow *et al*., 1989; Jurvelin *et al*., 1995) and US methods (Toyras *et al*., 2001; Zheng *et al*., 2006) have been employed by researchers to measure its thickness. As the ArtC is very thin, a complete piece of ArtC with underlying bone can be cut/ punched out. Two different layers of ArtC and bone can be differentiated under microscope. By using the device showed in Figure 9, tissue thickness of ArtC can be measured (Jurvelin *et al*., 1995). This method was also used for the calculation of Poisson's ratio by measuring the axial and lateral deformations caused by unconfined compression (Jurvelin *et al*., 1997). Generally, the hardness keeps increasing from the superficial zone of ArtC to underlying bone. Needle punching technique was also employed to determine the thickness of ArtC layer (Figure 10) (Swann and Seedhom, 1989). The correlation of the ArtC thickness measured by microscopic method and needle punching technique is relatively high (R^2 = 0.94) (Jurvelin *et al*., 1995). On the other hand, laser (Horikawa, *et al*., 1993), ultrasonic (Zheng and Mak, 1996; 1999; Zheng *et al*., 2000) and MRI (Gefen *et al*., 2001; Nieminen *et al*., 2004) methods have been used for determining thickness of skin, muscles and connective tissues in pervious studies.

When using US for tissue, thickness measurement, the speed of sound (SOS)

varies in various tissues. Different mean values of SOS for various mammal animal tissues were reported in a pervious study (Goss *et al*., 1980) and used for the US test in biological soft tissues. SOS was also studied for ArtC (Patil and Zheng, 2004; Zheng *et al*., 2006). As the SOS is easily affected by different parameters, US may cause relatively larger variations in the results compared with those obtained by other thickness measurement methods. Laser and MRI are mainly used for measuring tissue thickness of skin and muscular tissues. The limitations of using laser include superficial penetration of soft tissue and its safety concerns, whereas MRI is difficult in the differentiation of tissues boundaries in imaging, as mentioned earlier.

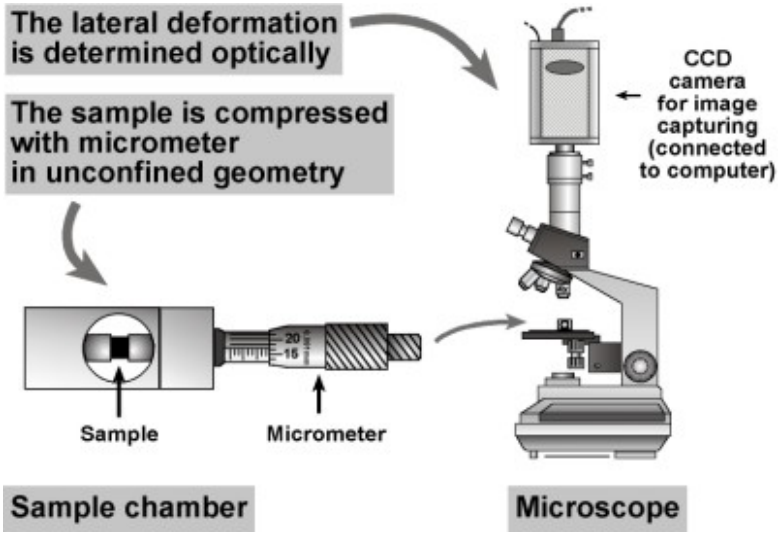

Figure 9 Device for thickness of deformation measurements and Poisson's ratio estimation of ArtC under microscope by unconfined compression (Jurvelin *et al*., 1997).

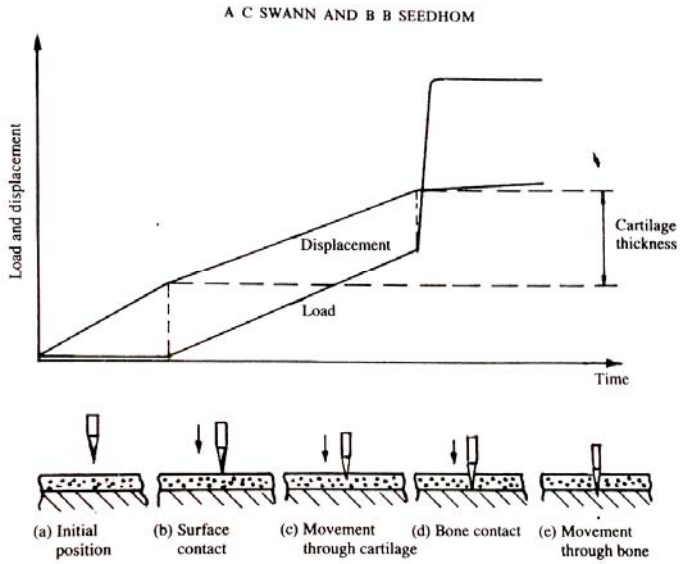

Figure 10 Diagram shows the needle punching technique used for thickness measurement of articular cartilage. By measuring different forces, which are used for punching through different layers of ArtC, the thickness of different layer can be measured. (Swann and Seedhom, 1989).

1.3.2.2 Indentation Force

Indentation force is another important parameter for calculating tissue properties using indentation tests. The force can be measured continuously via strain gauge (Mow *et al*., 1989; Swann and Seedhom, 1989; Zheng and Mak, 1996) and fiber optic sensor (Fleming and Beynnon, 2004). The strain gauge force sensor can be used in the material testing system (Mow *et al*., 1989; Swann and Seedom, 1989) and hand-held indentation probe. It can be placed uniaxially (Figure 11) (Zheng and Mak, 1996; Suh

et al., 2001) or mounted in parallel to the lateral border of the probe (Figure 12) (Han *et al*., 2003).

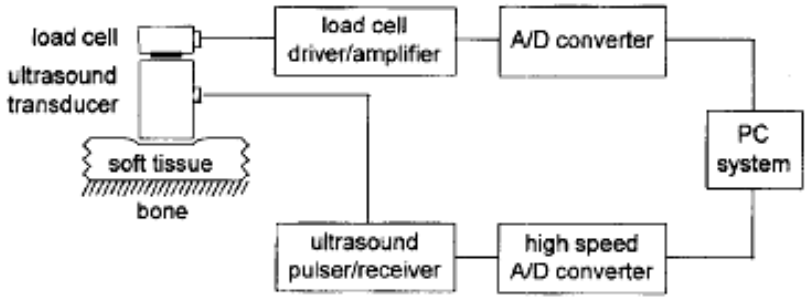

Figure 11 The schematic diagram of the ultrasound indentation system, the load cell was connected with ultrasound transducer uni-axially (Zheng and Mak, 1996).

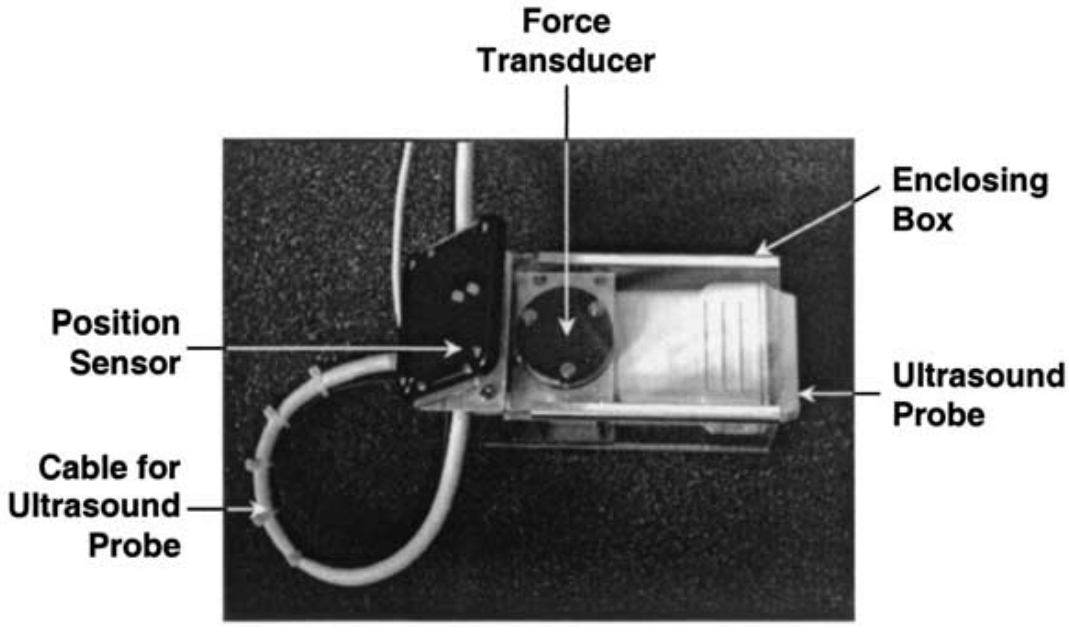

Figure 12 The B-mode ultrasound probe was mounted with 6-axis (3 normal and 3 shear stresses) force transducer laterally and 3D electromechanical position sensor (Han *et al*., 2003).

1.3.2.3 Poisson's Ratio

Traditionally, Poisson's ratio can be measured by using various methods including biphasic compression (Mow *et al*., 1989; Jurvelin *et al*., 1997), biphasic indentation (Mak *et al*., 1987; Mow *et al*., 1989) and uni-axial unconfined compression. As demonstrated in Figure 4, unconfined and confined compressions can be performed to measure Young's modulus E and aggregate modulus H_A, respectively. So, the Poisson's ratio of the solid phase v_s can be calculated by the following equation

$$H_A = \frac{E(1-\upsilon_s)}{(1-\upsilon_s)(1-2\upsilon_s)} \tag{14}$$

In Figure 6, the experimental results (curve in right hand side) from biphasic indentation can be compared with the master solution (curve in left hand side) to estimate the corresponding Poisson's ratio (Mak *et al*., 1987; Mow *et al*., 1989). Jurvelin *et al*. (1997) proposed a compressive device (Figure 9) for the ArtC and observed the axial and lateral deformation under microscope. Later, Fortin *et al*. (2003) proposed to use US approach (Figure 13) for monitoring the axial and lateral deformation during unconfined compression. Using high frequency US (50MHz), small deformation can be measured by this method. The Poisson's ratio measured by

biphasic compression and indentation is for the solid phase only. The Poisson's ratio for the single phasic indentation is conventionally assumed to be 0.42 to 0.50 for instantaneous response (Jurvelin *et al*., 1988; Kempson *et al*., 1971). So, the fluid is kept in the ECM due to inadequate time to be completely removed.

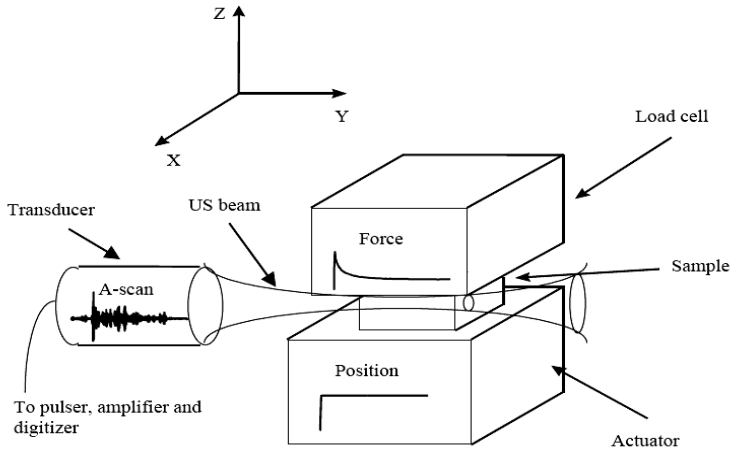

Figure 13 The schematic diagram of the setting for determining Poisson's ratio by monitoring axial and lateral deformation during unconfined compression using high frequency (50MHz) ultrasound transducer (Fortin *et al*., 2003).

Recently, a novel approach was reported to obtain Young's modulus and Poisson's ratio by double-indentation using two different sized indentors (Jin and Lewis, 2004). Using the two different sized indentors, two different sets of force and deformation data can be obtained for estimating the Poisson's ratio. In the single phasic model, equation (3) can be rearranged to form a nonlinear equation as follows,

$$\frac{P_1/w_1}{P_2/w_2}=\frac{a_1}{a_2}\cdot\frac{\kappa(a_1/h,\upsilon)}{\kappa(a_2/h,\upsilon)} \tag{15}$$

Where the indentation load *P*, deformation *w* and the indentor radius *a* can be obtained during indentation. Therefore, Poisson's ratio in the kappa factor is the only unknown in equation (15), which can be modified to

$$f(a_1/h,a_2/h,\upsilon)=\frac{P_1 w_2 a_2}{P_2 w_1 a_1} \tag{16}$$

The function *f* of the left hand side of equation (16) can be calculated from the kappa table by Hayes (Hayes *et al*., 1972) by finding the ratio of two kappa factors with same Poisson's ratio *v* but different aspect ratio *a*/*h* according to different indentor radii a_1 and a_2.

The advantage of this novel approach is that no additional separate test is required to be carried out for determining the Poisson's ratio. So, Poisson's ratio can be obtained conveniently instead of making any assumptions. Therefore, the accuracy for measuring mechanical properties of soft tissue can be improved. However, this method is based on the assumption of the infinitesimal deformation, which is not practical to be obtained in manual indentation. The small corresponding indentation

load used for infinitesimal deformation is not easy to be monitored by currently available sensors. So, the effects of the finite deformation on the estimation of Poisson's ratio and Young's modulus by double-indentation with two different sized indentors cannot be fully understood.

1. 4 Objectives of the Study

In order to obtain the mechanical properties of soft tissue by an in-vivo test, single phasic indentation was selected in this study rather than other methods or models due to its simplicity and simple experimental setup, which is feasible for *in-vivo* test. As reviewed in last section, Poisson's ratio used for the calculation of Young's modulus in single phasic indentation is conventionally assumed or separately measured by an additional test.

Therefore, the aim of this study was to develop calculation algorithms for single phasic indentation to estimate the Young's modulus and Poisson's ratio simultaneously for estimating mechanical properties of soft tissue more accurately and comprehensively.

To realize this aim, there were following specific objectives:

1. to study the finite deformation effects on the estimation of Young's modulus and Poisson's ratio by double-indentation with two different sized indentors and

develop a compensation measure;

2. to develop several calculation strategies for estimating Young’s modulus and Poisson’s ratio of soft tissue simultaneously by single-indentation;
3. to verify the effectiveness of the algorithms for estimating Young’s modulus and Poisson’s ratio of soft tissue using finite element analysis;
4. to test the effectiveness of those novel algorithms for estimating Young’s modulus and Poisson’s ratio of soft tissue by silicone phantom study;
5. to demonstrate the feasibility of using the novel algorithms for the measurement of articular cartilage.

Chapter 2 Methods for the Estimation of Poisson's Ratio and Young's Modulus simultaneously

In this chapter, there different methods are introduced to estimate Poisson's ratio and Young's modulus simultaneously using indentation data. First, the double-indentation method proposed by Jin and Lewis (2004) was improved by considering the finite deformation accrued in the practical application. Then, we proposed two novel algorithms to extract Poisson's ratio and Young's modulus simultaneously from single-indentation data.

2.1 Double-Indentation using Different Sized Indentors

As introduced in section 1.3.1 Indentation model, the rigorous indentation model proposed by Hayes *et al.* (1972) can only be applied for infinitesimal deformation. The double-indentation method proposed by Jin and Lewis (2004) was based on Hayes' solution (equation 3). Zhang *et al.* (1997) reported a set of kappa values with consideration of the finite deformation using finite element analysis (FEA) (Zhang *et al.*, 1997). The effects of finite deformation can be compensated by including a deformation-dependent kappa value in the calculation. In order to study the effects of finite deformation on the double-indentation method, the deformation-dependent kappa obtained by Zheng *et al.* (1997) was included in Jin and Lewis's algorithm (equation 16) to form the following equation,

$$g(a_1/h, a_2/h, w/h, v) = \frac{\kappa(a_1/h, w/h, v)}{\kappa(a_2/h, w/h, v)} = \frac{P_1 w_2 a_2}{P_2 w_1 a_1} \quad (17)$$

where $g(a_1/h, a_2/h, w/h, v)$ is the ratio between two kappa values with the same Poisson's ratio and deformation ratio but different aspect ratios. a_1 and a_2 are the radius of indentors, h is the tissue thickness, P_1 and P_2 are the indentation loads, w_1 and w_2 are two corresponding deformations, *and* v is the Poisson's ratio, respectively. In equation (17), Poisson's ratio v is the only unknown in the function $g(a_1/h, a_2/h, w/h, v)$ when h, a_1, a_2, and w are determined in a double-indentation test. Therefore, v can be calculated from the value of $(P_1 w_2 a_2)/(P_2 w_1 a_1)$, which can be obtained in a double-indentation test. More detailed descriptions of the calculation are introduced in next chapter using some specific parameters.

2.2 Single-Indentation with Two Different Deformations

Double-indentation can be used to estimate the Poisson's ratio of soft tissue. However, time should be given for tissue relaxation after first indentation due to the viscoelastic properties of the biological tissues. Moreover, during the period of tissue relaxation, biological changes of tissue may happen, including fluid and ions movements, which may affect the mechanical properties of tissue. In order to reduce the experimental duration, a novel method to estimate Poisson's ratio and Young's modulus simultaneously by a single-indentation test was proposed in this study. During single-indentation, the data of corresponding force can be extracted at different deformations, which can be expressed as follow:

$$E = \frac{(1-v^2)}{2a\kappa(a/h, w_1/h, v)}\frac{P_1}{w_1} \tag{18}$$

and

$$E = \frac{(1-v^2)}{2a\kappa(a/h, w_2/h, v)}\frac{P_2}{w_2} \tag{19}$$

The forces P_1 and P_2 in equations (18) and (19) correspond to the deformations, w_1 and w_2, respectively. Combining equations (18) and (19) yields

$$\frac{(1-v^2)}{2a\kappa(a/h, w_1/h, v)}\frac{P_1}{w_1} = \frac{(1-v^2)}{2a\kappa(a/h, w_2/h, v)}\frac{P_2}{w_2} \tag{20}$$

and can be rearranged into

$$\frac{P_1}{w_1}\frac{w_2}{P_2} = \frac{\kappa(a/h, w_1/h, v)}{\kappa(a/h, w_2/h, v)} \tag{21}$$

and further into

$$f(a/h, w_1/h, w_2/h, v) = \frac{P_1 w_2}{P_2 w_1} \tag{22}$$

where $f(a/h, w_1/h, w_2/h, v)$ at left hand side in equation (22) is the ratio between two kappa values with the same Poisson's ratio v and aspect ratio a/h but different deformation ratios. As the indentor radius a, tissue thickness h, indentation loads P_1 and P_2, and the corresponding deformations w_1 and w_2 can be measured during indentation, the Poisson's ratio v can be estimated by solving the function $f(a/h, w_1/h, w_2/h, v)$ in equation (22). After obtaining v, E can be calculated using

either equation 18 or 19.

2.3 Single-Indentation using Deformation-Dependent Indentation Stiffness

The single-indentation method introduced in last section uses data of two different deformation points. In this section, another algorithm was proposed for estimating Poisson's ratio and Young's modulus of soft tissue simultaneously using multiple deformation points of a single indentation test. In this proposed algorithm, the relationship between the Poisson's ratio and the deformation-dependent indentation stiffness was established. By including the effect of finite deformation for indentation, Equation (4) can be rearranged to

$$\frac{P}{w} = \frac{2 \cdot a \cdot E \cdot \kappa_n\left(a/h, w/h, v\right)}{\left(1 - v^2\right)}. \tag{23}$$

According to the results of Zhang *et al*. (1997) obtained by the non-linear finite element analysis, it was found that κ_n almost linearly depends on the deformation *w*. Therefore, κ_n can be written as

$$\kappa_n\left(a/h, w/h, v\right) = \kappa\left(a/h, v\right) \cdot \left(1 + \beta\, w/h\right) \tag{24}$$

where β is a factor that depends on the aspect ratio and Poisson's ratio, $\kappa\left(a/h, v\right)$ is the scaling factor in the indentation equation (3) proposed by Hayes *et al*. (1972) for an infinitesimal deformation. Table of β factor for different aspect ratios *a*/*h* (0.2 ~ 2) and Poisson's ratios *v* (0.1 ~ 0.5) can then be established according to the result of κ_n (Zhang *et al.*, 1997), as shown in Table 1. This β table (Table 1) can be used to

estimate the Poisson's ratio during indentation tests. By substituting equation (24) into equation (23), the deformation-dependent indentation stiffness can be written as

$$\frac{P}{w} = \frac{2aE\kappa(a/h, v)}{1-v^2}(1 + \beta \cdot w/h) \tag{25a}$$

It can be rewritten as

$$P/w = c + c\beta \cdot w/h\,. \tag{25b}$$

by defining

$$c = \frac{2aE\kappa(a/h, v)}{1-v^2} \tag{26}$$

According to Equation (25b), c can be obtained as the y-intercept of the linear regression of a sequence of indentation data P/w and w/h. The slope of the liner relationship between P/w and w/h is $c\beta$. Therefore, β can be obtained using the experimental data, i.e. β = slope / y-intercept. Since the relationship between Poisson's ratio v and β for certain aspect ratio a/h has already been established (Table 1), the Poisson's ratio can be estimated using the single-indentation data. After v is obtained, E

Table 1 The β table for different aspect ratios and Poisson's ratios.

	Aspect ratio (*a*/*h*)						
Poisson's ratio (*v*)	**0.2**	**0.4**	**0.6**	**0.8**	**1.0**	**1.5**	**2.0**
0.10	0.012	0.014	0.012	0.016	0.004	0.222	0.286
0.20	0.012	0.014	0.023	0.034	0.098	0.284	0.338
0.30	0.035	0.037	0.073	0.208	0.271	0.421	0.466
0.35	0.179	0.141	0.215	0.373	0.478	0.559	0.595
0.40	0.301	0.265	0.401	0.597	0.728	0.810	0.838
0.45	0.554	0.519	0.740	1.012	1.002	1.271	1.327
0.50	0.946	0.920	1.295	1.551	1.478	2.550	2.897

Chapter 3 Finite Element Study

Finite element (FE) analysis has been widely used in mechanical engineering and materials science. Using FE analysis, the feasibility of the proposed methods for calculating Poisson's ratio presented in Chapter 2 could be investigated before further experiments on phantoms and articular cartilage. FE analysis may help to neglect the effects of uncontrolled experimental errors in practical experiment.

In this study, FE models were established for studying the effects of finite deformation on the estimation of Poisson's ratio using double-indentation and testing the feasibility of estimating Poisson's ratio and Young's modulus simultaneously using single-indentation.

3.1 FE Models

Axisymmetric solid FE models were established using ABAQUS/CAE package (Version 6.4, Hibbitt, Karlsson & Sorensen, Inc, US) to simulate double-indentation with two different sized, rigid, cylindrical, flat-ended indentors (Figure 14). These FE models were firstly used for studying the effects of finite deformation on the calculation using double-indentation. Then, those models were employed for estimating Poisson's ratio and Young's modulus using single-indentation methods. The radii of indentors were set to be 4.5 mm and 9.0 mm. The thickness and radius of soft tissue in the FE model were set to be 4.5 mm and 45 mm, respectively. So, the aspect ratios of these two models were 1.0 and 2.0. As the radius of the specimen was at least 5 times longer than that of indentor, the boundary condition of the specimen in the lateral border could be neglected during indentation (Spilker *et al.,* 1992).

These FE models were meshed by four-node bilinear elements (CAX4) with the 0.50 x 0.50 mm^2 grid density. Comparisons among the 0.45 x 0.45 mm^2, 0.50 x 0.50 mm^2 and 0.90 x 0.90 mm^2 had been carried out before selecting 0.50 x 0.50 mm^2 as grid density (Choi and Zheng, 2005). Zhang *et al.* (1997) reported that there is no statistically significant difference (0.3%) between the results of using the element with the grid density 0.50 x 0.50 mm^2 compared with 0.30 x 0.30 mm^2. The material properties of the indentor were assigned to be 100 GPa and 0.49 for Young's modulus and Poisson's ratio, respectively, for ensuring adequate rigidity (Zhang *et al*., 1997). The Young's modulus of the soft tissue was assigned to be 60 kPa and Poisson's ratio varied from 0.30 to 0.499 (value of 0.50 cannot be set due to the limitation of the FEA software) (Hayes *et al*., 1972). In this model, the friction force between the surfaces of the indentor and the tissue was ignored. Also, it was assumed that the soft tissue was fixed on a rigid substrate.

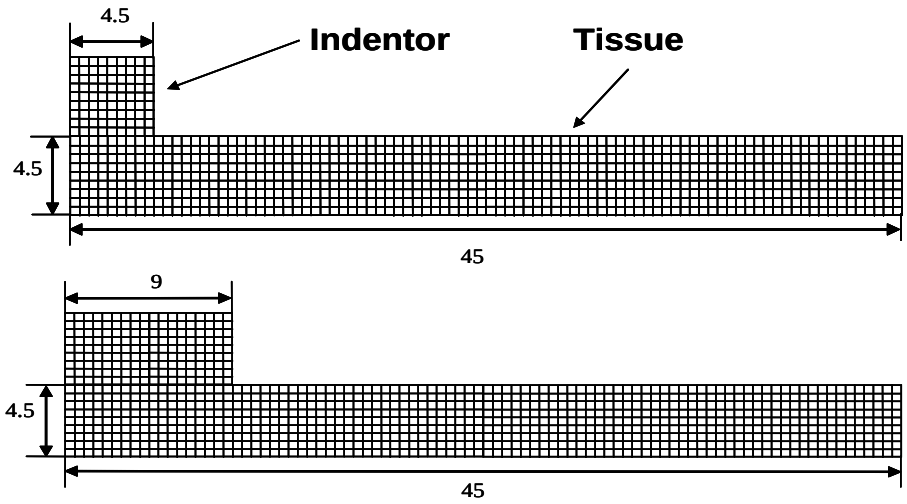

Figure 14 FE meshed model for the indentation of soft tissues. For the upper model, the aspect ratio (ratio between indentor and tissue thickness, *a*/*h*) was set as 1.0. For the lower model, the aspect ratio was set as 2.0. The radius of specimen was set at least 5 times longer than the radius of indentors. The grid density of mesh was set as 0.5 x 0.5 mm^2.

In FE simulation, the displacement was given to the nodes on the upper surface of the indentor. The deformation ratio *w*/*h* was defined to be the ratio of indentation depth and the tissue thickness. The corresponding reaction force was recorded as the indentation load in every time step. The total deformation ratio was set to be 15 % of tissue thickness and applied in 150 time steps. The force-deformation data extracted from the first 10 % was used for calculation in this study.

3.2 Effects of Finite Deformation in Double-Indentation

3.2.1 Methods

The indentation loads were extracted during the corresponding deformation ratios (0.1%, 2.5%, 5%, 7.5% and 10%) and used to calculate the function $g(a_1/h, a_2/h, w/h, \upsilon)$, which is the ratio between two kappa values with the same Poisson's ratio and deformation ratio by equation (17). Firstly, the kappa table for infinitesimal indentation (Hayes *et al.*, 1972) was applied to develop the nonlinear relationship between Poisson's ratio and the ratio of two kappa values with different aspect ratios (a_1/h and a_2/h = 1.0 and 2.0) (Figure 15). Then, the kappa table with considering the finite deformation was applied to develop other nonlinear relationships with respect to various deformations (0.1%, 5.0% and 10%) (Figure 16). Therefore, the nonlinear relationships between Poisson's ratio and ratio between two kappa values with different aspect ratios were used to calculate the Poisson's ratio. The force-deformation data of corresponding deformation was extracted to estimate the Poisson's ratio via interpolation between the known data points of these nonlinear relationships. Consequently, the estimated Poisson's ratio was used to calculate Young's modulus by equation (4).

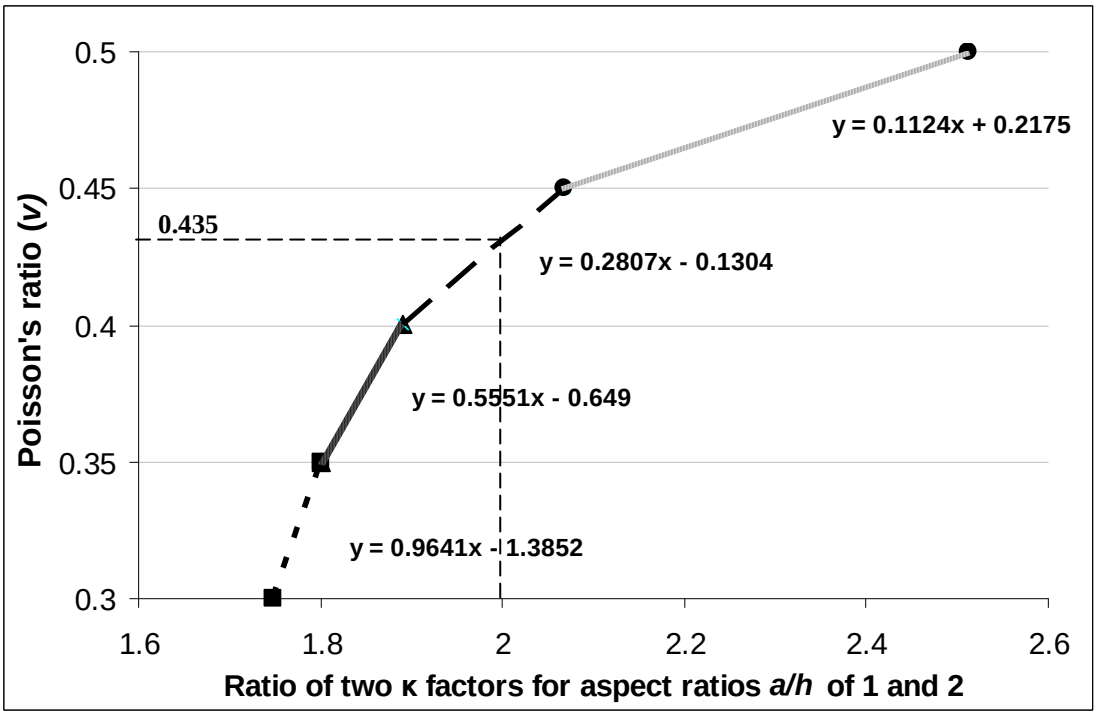

Figure 15 The non-linear relationship between Poisson's ratio v and ratio of two kappa values for infinitesimal indentation calculated from Hayes's data, i.e. $\kappa(a_1/h,\upsilon)/\kappa(a_2/h,\upsilon)$. Radius of indentors ($a_1$ and a_2) was set to be 4.5 mm and 9.0 mm, respectively. The thickness h was set as 4.5 mm. Linear interpolations between two known data points can be used to estimate the Poisson's ratio. The ratio of two κ factors (2.0) for aspect ratios a/h of 1 and 2 was used to estimate the Poisson's ratio and the result was 0.435.

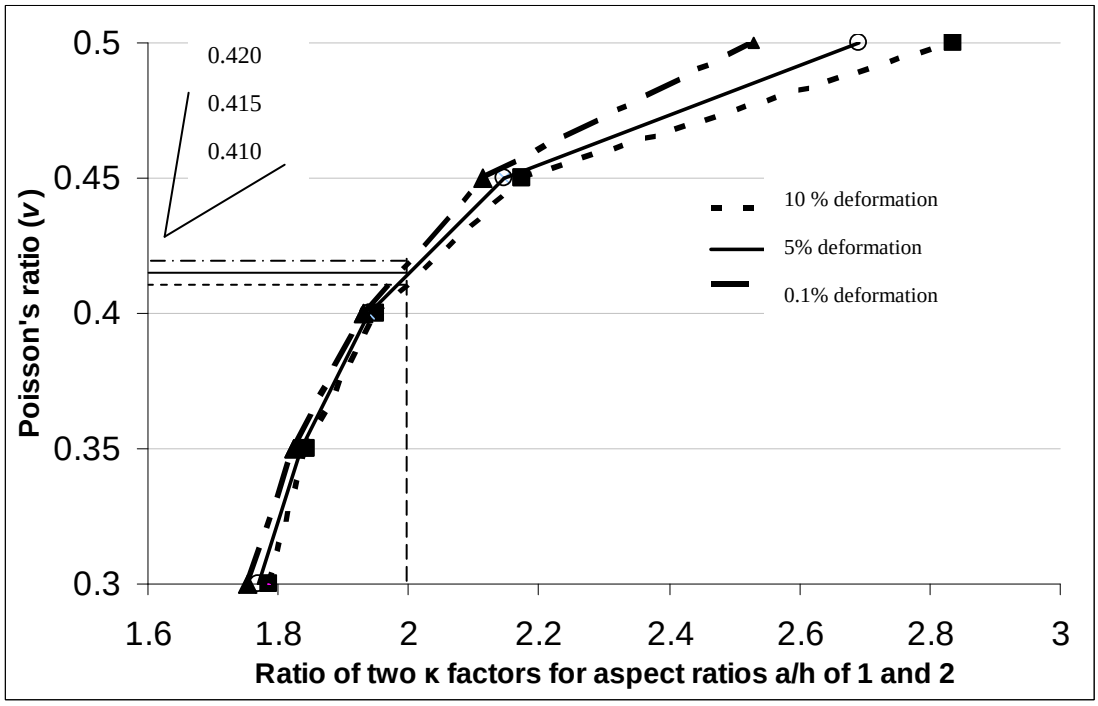

Figure 16 The non-linear relationship between Poisson's ratio v and ratio of two kappa values with different indentation deformations calculated from Zhang's data, i.e. $\kappa(a_1/h,\upsilon)/\kappa(a_2/h,\upsilon)$. Radius of indentors ($a_1$ and a_2) was set to be 4.5 mm and 9.0 mm, respectively. The thickness h was set as 4.5 mm. The ratio of two κ factors (2.0) for aspect ratios a/h of 1 and 2 was used to estimate the Poisson's ratio with respect to different deformation. The estimated Poisson's ratio is around 0.41 to 0.42 after considering the effects of finite deformation.

3.2.2 Results

The force - deformation data was extracted from the FE simulation (Figure 17) for calculating the function $g(a_1/h, a_2/h, w/h, \upsilon)$ by equation (17). Table 2 showed the comparison of the Poisson's ratio obtained from the force - deformation data of the FE simulation with and without considering the effects of finite deformation. The

Poisson's ratios obtained without considering the effects of finite deformation were slightly larger than the preset values in FE model, with an overall means of estimation error of 2.77% ± 2.14%.

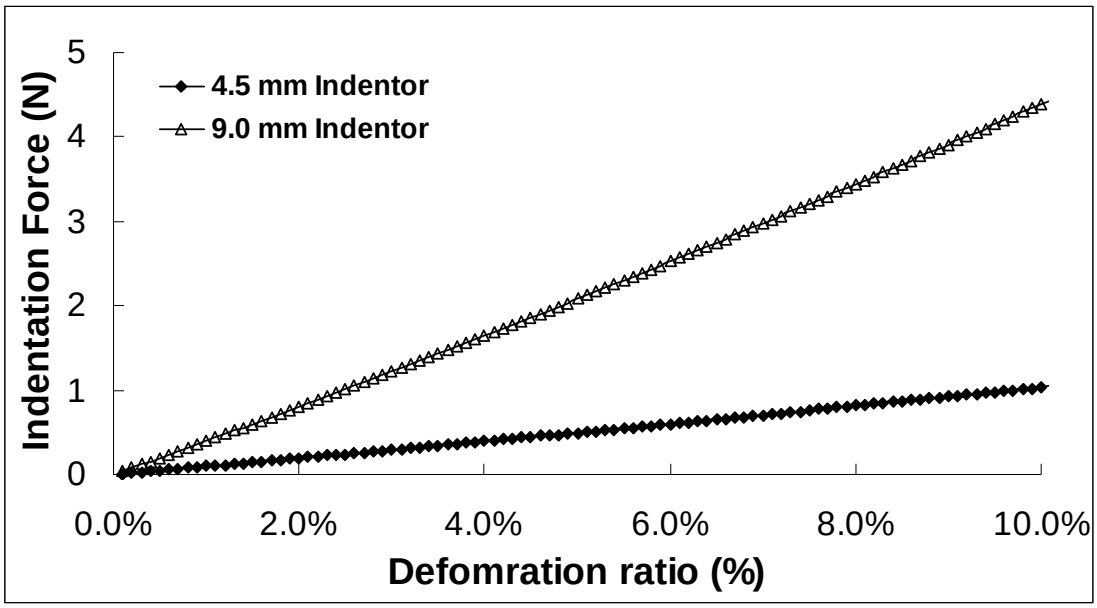

Figure 17 Force – deformation curve extracted from FE simulation of the indentation using different sized indentors.

Table 2 Comparison of Poisson's ratios obtained with and without considering the effects of finite deformation (Young's modulus of tissue in FE model is 60kPa, the Poisson's ratios range from 0.3 to 0.5).

True Poisson's ratios (v)	Deformation Ratios (w/h)	Estimated Poisson's Ratios (v)			
		Without considering large deformation effects	Estimation errors (%)	With considering large deformation effects	Estimation errors (%)
0.30	0.1%	0.305	1.76%	0.299	-0.36%
	2.5%	0.310	3.28%	0.291	-3.07%
	5.0%	0.318	5.96%	0.290	-3.23%
	7.5%	0.326	8.76%	0.291	-3.02%
	10.0%	0.335	11.73%	0.293	-2.20%
0.35	0.1%	0.353	0.96%	0.337	-3.69%
	2.5%	0.356	1.58%	0.336	-4.08%
	5.0%	0.360	2.82%	0.337	-3.69%
	7.5%	0.364	4.12%	0.339	-3.15%
	10.0%	0.369	5.53%	0.342	-2.35%
0.40	0.1%	0.402	0.53%	0.385	-3.82%
	2.5%	0.403	0.84%	0.384	-3.94%
	5.0%	0.406	1.40%	0.386	-3.55%
	7.5%	0.408	1.99%	0.388	-3.12%
	10.0%	0.411	2.64%	0.390	-2.60%
0.45	0.1%	0.451	0.28%	0.441	-2.03%
	2.5%	0.452	0.44%	0.439	-2.49%
	5.0%	0.453	0.75%	0.439	-2.53%
	7.5%	0.455	1.06%	0.439	-2.54%
	10.0%	0.456	1.38%	0.439	-2.53%
0.50	0.1%	0.501	0.30%	0.500	-0.03%
	2.5%	0.507	1.31%	0.496	-0.81%
	5.0%	0.512	2.38%	0.493	-1.35%
	7.5%	0.517	3.41%	0.492	-1.66%
	10.0%	0.520	4.08%	0.489	-2.17%

After obtaining the Poisson’s ratios as shown in Table 2, the Young’s modulus was estimated by equation (4) using both force - deformation pairs in the FE model with two different aspect ratios (1.0 and 2.0). It could be observed from Table 2 that the estimation errors of estimated Poisson’s ratio with and without considering finite deformation ranged from -0.03% to -4.08% and 0.28% to 11.73%, respectively. Tables 3 and 4 show the comparisons of Young’s modulus with and without considering the effects of finite deformation. The Young’s modulus obtained without considering the effects of finite deformation during indentation increased with deformation. It was noted that estimation errors of estimated Young’s modulus with and without considering finite deformation ranged from -0.05% to 4.81% and -0.01% to 22.75%, respectively.

Table 3 The comparison of Young's modulus (*E*) estimated by Poisson's ratio with and without considering the effects of finite deformation (Young's modulus of tissue in FE model is 60 kPa, the Poisson's ratios vary from 0.3 to 0.5 and aspect ratio = 1.0).

True Poisson's ratios (*v*)	**Deformation Ratios (*w/h*)**	**Estimated *E* (kPa)**	**Estimation error (%)**	**Estimated *E* (kPa)**	**Estimation error (%)**
		Without considering large deformation effects		**With considering large deformation effects**	
0.30	0.1%	59.99	-0.01%	59.19	-1.34%
	2.5%	60.21	0.35%	59.52	-0.80%
	5.0%	60.17	0.29%	59.43	-0.94%
	7.5%	60.10	0.16%	59.30	-1.17%
	10.0%	59.97	-0.05%	59.08	-1.53%
0.35	0.1%	60.06	0.11%	60.42	0.71%
	2.5%	60.58	0.97%	60.42	0.70%
	5.0%	60.87	1.46%	60.16	0.26%
	7.5%	61.14	1.89%	59.86	-0.24%
	10.0%	61.35	2.25%	59.50	-0.83%
0.40	0.1%	60.14	0.23%	61.32	2.19%
	2.5%	61.00	1.66%	61.22	2.03%
	5.0%	61.71	2.85%	60.89	1.49%
	7.5%	62.39	3.98%	60.55	0.92%
	10.0%	63.02	5.03%	60.16	0.27%
0.45	0.1%	60.18	0.31%	61.33	2.21%
	2.5%	61.65	2.76%	61.54	2.57%
	5.0%	62.97	4.95%	61.47	2.45%
	7.5%	64.28	7.13%	61.38	2.31%
	10.0%	65.53	9.21%	61.25	2.09%
0.50	0.1%	60.37	0.61%	60.86	1.43%
	2.5%	62.35	3.91%	61.43	2.39%
	5.0%	64.42	7.36%	61.96	3.27%
	7.5%	66.52	10.86%	62.43	4.05%
	10.0%	68.68	14.47%	62.89	4.81%

Table 4 The comparison of Young's modulus (*E*) estimated by Poisson's ratio with and without considering the effects of finite deformation (Young's modulus of tissue in FE model is 60 kPa, the Poisson's ratios vary from 0.3 to 0.5 and aspect ratio = 2.0).

True Poisson's ratios (*v*)	Deformation Ratios (*w/h*)	Estimated *E* (kPa) Without considering large deformation effects	Estimation error (%) Without considering large deformation effects	Estimated *E* (kPa) With considering large deformation effects	Estimation error (%) With considering large deformation effects
0.30	0.1%	60.16	0.27%	59.18	-1.37%
	2.5%	60.55	0.91%	59.39	-1.02%
	5.0%	60.79	1.32%	59.30	-1.16%
	7.5%	61.02	1.70%	59.18	-1.36%
	10.0%	61.20	2.01%	59.00	-1.66%
0.35	0.1%	60.26	0.43%	59.83	-0.29%
	2.5%	60.91	1.51%	59.78	-0.36%
	5.0%	61.47	2.45%	59.61	-0.65%
	7.5%	62.01	3.36%	59.42	-0.96%
	10.0%	62.53	4.22%	59.20	-1.34%
0.40	0.1%	60.36	0.59%	60.28	0.47%
	2.5%	61.36	2.26%	60.17	0.28%
	5.0%	62.34	3.89%	59.95	-0.09%
	7.5%	63.30	5.51%	59.72	-0.46%
	10.0%	64.25	7.08%	59.48	-0.87%
0.45	0.1%	60.52	0.87%	60.35	0.58%
	2.5%	62.19	3.65%	60.29	0.48%
	5.0%	63.90	6.50%	60.12	0.20%
	7.5%	65.61	9.35%	59.97	-0.05%
	10.0%	67.30	12.16%	59.81	-0.32%
0.50	0.1%	60.69	1.15%	60.81	1.35%
	2.5%	63.80	6.33%	60.50	0.83%
	5.0%	67.13	11.89%	60.28	0.47%
	7.5%	70.54	17.57%	60.13	0.22%
	10.0%	73.65	22.75%	59.73	-0.45%

3.2.3 Summary

From the above results, it was found that the finite deformation effects on the calculation of double-indentation were more obvious in the estimation of Young's modulus rather than that of Poisson's ratio. The errors during the estimation of Young's modulus without considering the finite deformation effects generally increased with the increase of Poisson's ratio (from 0.30 to 0.50) and deformation ratio (0.1% to 10%) under both aspect ratios (1.0 and 2.0). Moreover, the effects of this compensation were more obvious when the aspect ratio of indentation was larger. It might be due to the larger substrate effects in the thin tissue layer. In fact, the biological tissue might be relatively thin in many situations, the compensation using kappa factors might help to improve the accuracy of the calculation. However, it was revealed that the kappa factors (Zhang *et al*., 1997) could not totally compensate the finite deformation effects.

3.3 Estimation of Young's Modulus and Poisson's Ratio by Single-Indentation with Two Different Deformations

3.3.1 Methods

As mentioned in previous chapter, the advantage of the single-indentation over the double-indentation is that the experimental errors caused by the differences in settings, probe orientation and indentor misalignment between two indentations, could be avoided. FE models were built to investigate the feasibility for the simultaneous estimation of the Poisson's ratio and Young's modulus using the proposed single-indentation methods. The estimated Poisson's ratio and Young's modulus were compared with the assigned material properties of the FE models. The

Poisson's ratio and Young's modulus of the tissue model were assumed to be 0.45 and 60 kPa, respectively. The radius of the indentor in the FE models was set as 4.5 mm. FE models were established with various aspect ratios of 0.6, 0.8, 1.0, 1.5 and 2.0, respectively.

The force - deformation data was extracted at different deformation ratios (0.1%, 2.5%, 5.0% and 10.0%) and further used for estimating the Poisson's ratio and Young's modulus using equation (24). The ratios between two kappa values with two different deformations were formed as follows:

$$f_1 = \kappa(a/h, 2.5\%, v)/\kappa(a/h, 0.1\%, v) \tag{26}$$

$$f_2 = \kappa(a/h, 5\%, v)/\kappa(a/h, 0.1\%, v) \tag{27}$$

$$f_3 = \kappa(a/h, 10\%, v)/\kappa(a/h, 0.1\%, v) \tag{28}$$

The Poisson's ratio was then estimated using equations (26)-(28). Figures 18 and 19 showed the nonlinear relationships between Poisson's ratios and the ratio of two kappa values with a selected Poisson's ratio *v* and aspect ratio *a/h* but different deformation ratios $f(a/h, w_1/h, w_2/h, v)$. The aspect ratios in Figures 18 and 19 were set to be 0.6 and 1.5, respectively. Table 5 showed the conversion table between Poisson's ratios and ratios between two kappa values with two different deformation ratios when the aspect ratios ranged from 0.6 to 2.0.

After estimating the Poisson's ratio, the Young's modulus could be obtained using either equation (18) or (19) with the kappa value with deformation ratio 2.5%, 5.0% and 10.0%, respectively. Then, the estimated Poisson's ratio and Young's modulus under different deformation ratios were used to compare with the assigned

mechanical properties of the FE models for verifying the feasibility of this method.

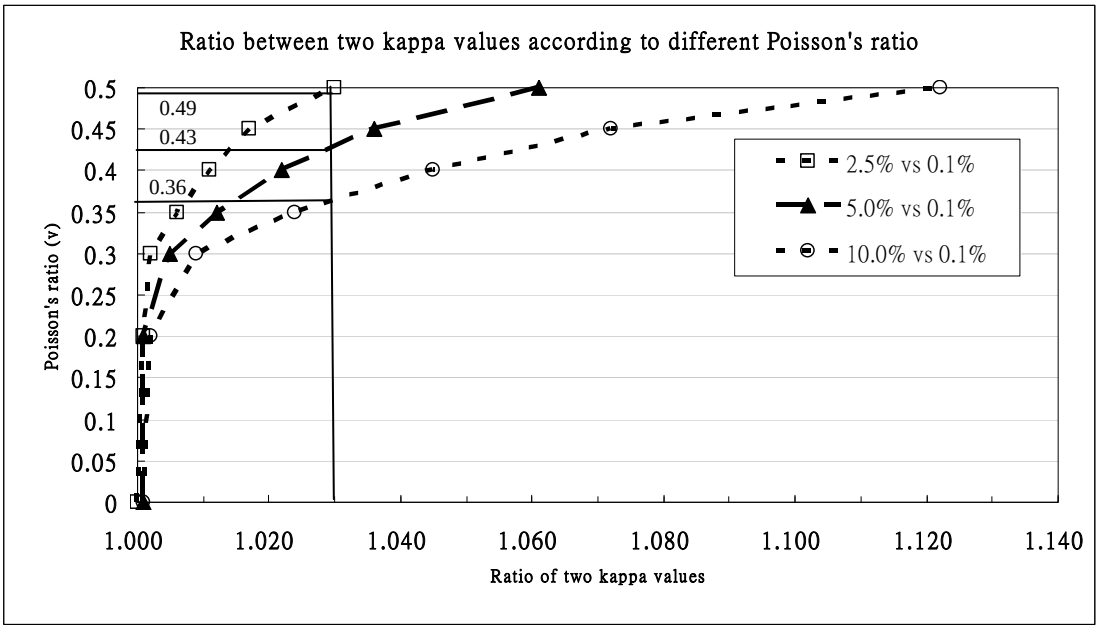

Figure 18 Nonlinear relationships of Poisson's ratio and the ratios between two kappa values with two different deformations. The aspect ratio in this case was set to be 0.6.

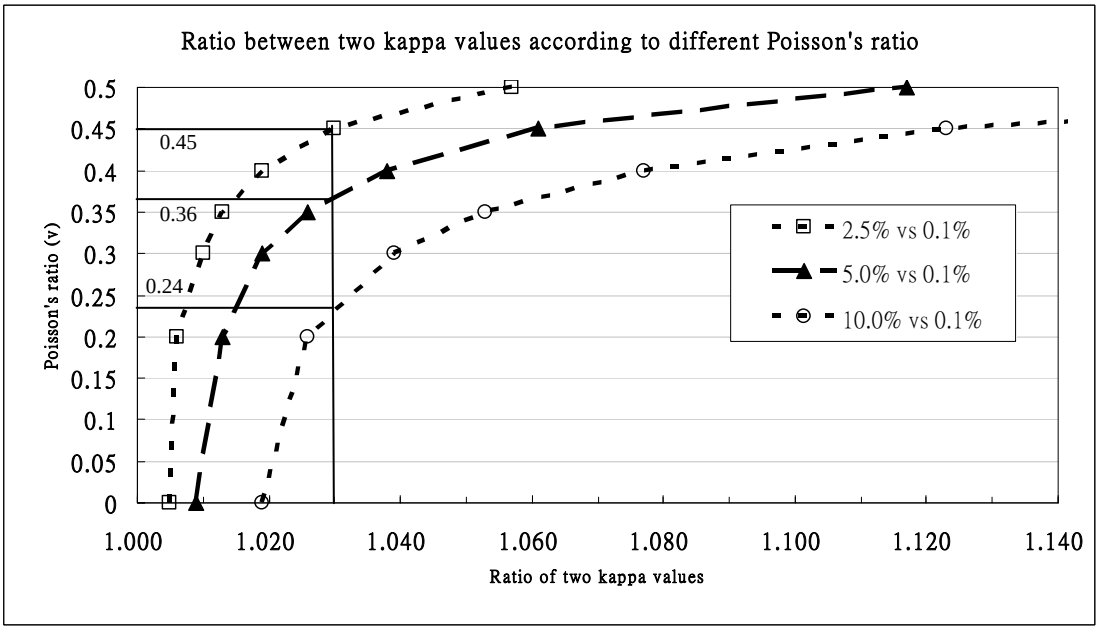

Figure 19 Nonlinear relationships of Poisson's ratio and the ratios between two kappa values with two different deformations. The aspect ratio in this case was set to be 1.5.

Table 5 The conversion table of Poisson's ratios against the ratios between two kappa values (i.e. $\kappa(a/h,\nu,2.5\%)/\kappa(a/h,\nu,0.1\%)$, $\kappa(a/h,\nu,5\%)/\kappa(a/h,\nu,0.1\%)$ and $\kappa(a/h,\nu,10\%)/\kappa(a/h,\nu,0.1\%)$) with various aspect ratios (0.6, 0.8, 1.0, 1.5 and 2.0).

	***ν* = 0.10**	**0.20**	**0.30**	**0.35**	**0.40**	**0.45**	**0.50**
***a/h* = 0.6**							
2.5%/0.1%	1.000	1.001	1.002	1.006	1.011	1.017	1.030
5%/0.1%	1.001	1.001	1.005	1.012	1.022	1.036	1.061
10%/0.1%	1.001	1.002	1.009	1.024	1.045	1.072	1.122
***a/h* = 0.8**							
2.5%/0.1%	1.000	1.001	1.005	1.009	1.015	1.025	1.033
5%/0.1%	1.000	1.002	1.011	1.019	1.031	1.051	1.068
10%/0.1%	1.001	1.004	1.022	1.039	1.063	1.102	1.138
***a/h* = 1.0**							
2.5%/0.1%	1.000	1.003	1.008	1.013	1.019	1.024	1.035
5%/0.1%	1.001	1.005	1.016	1.027	1.038	1.048	1.071
10%/0.1%	1.001	1.011	1.033	1.055	1.077	1.097	1.144
***a/h* = 1.5**							
2.5%/0.1%	1.005	1.006	1.010	1.013	1.019	1.030	1.057
5%/0.1%	1.009	1.013	1.019	1.026	1.038	1.061	1.117
10%/0.1%	1.019	1.026	1.039	1.053	1.077	1.123	1.235
***a/h* = 2.0**							
2.5%/0.1%	1.006	1.008	1.011	1.014	1.020	1.031	1.065
5%/0.1%	1.013	1.016	1.022	1.028	1.040	1.063	1.133
10%/0.1%	1.026	1.032	1.044	1.057	1.080	1.128	1.268

3.3.2 Results

Figure 20 showed that the force - deformation curve obtained from the indentation simulated by FE analysis. Table 6 showed the estimated Poisson's ratios, which were obtained by different ratios between two kappa values with different deformation ratios (equations 26-28), ranging from 0.431 to 0.444 when the aspect ratios ranged from 0.6 to 2.0. The percentage errors of the estimated Poisson's ratio compared with the assigned Poisson's ratio (ν = 0.45) ranged from -1.27 % to – 8.14 %.

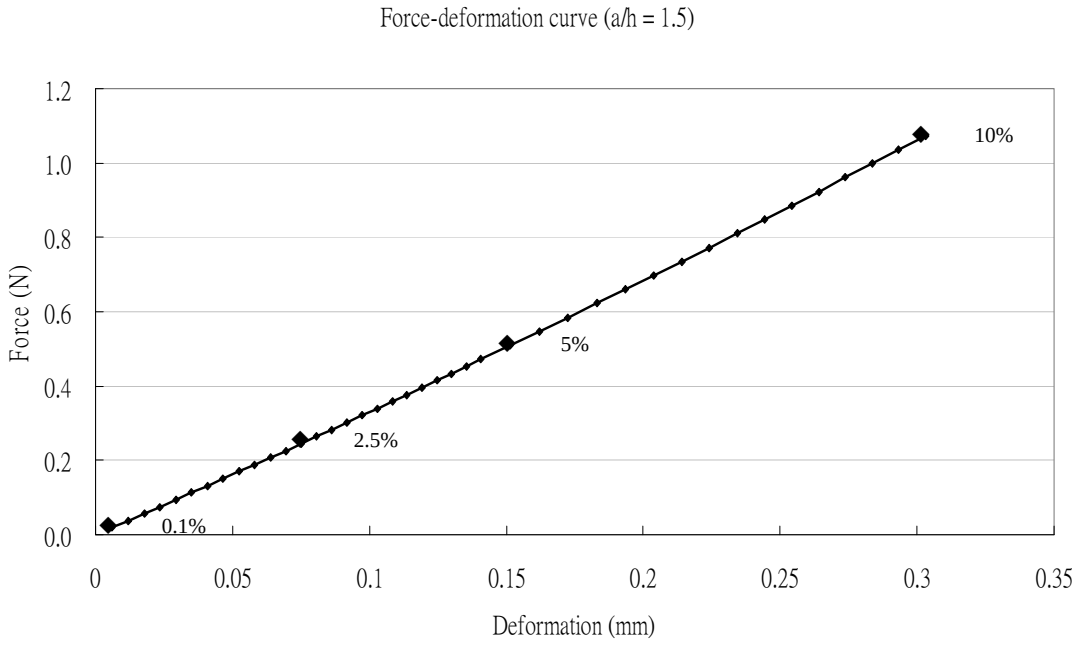

Figure 20 The force - deformation curve obtained from the FE simulation. The tissue thickness was set to be 3 mm and the maximal deformation ratio was limited to 10 %. The aspect ratio was set to be 1.5.

Table 6 Comparison between estimated Poisson's ratios obtained using proposed method and the assigned value used in FE model (indentor radius = 4.5 mm, Young's modulus = 60 kPa and Poisson's ratio = 0.45).

	a/h = 0.6	**0.8**	**1.0**	**1.5**	**2.0**
2.5%/0.1%	0.427	0.422	0.443	0.443	0.443
5.0%/0.1%	0.412	0.418	0.440	0.443	0.445
10.0%/0.1%	0.401	0.414	0.444	0.444	0.446
Average	0.413	0.418	0.442	0.444	0.444
Percentage error	-8.14%	-7.12%	-1.73%	-1.42%	-1.27%

The estimated Poisson's ratios were used to further estimate the Young's modulus using equation (4). Table 7 showed the means and percentage errors of Young's modulus. The Young's modulus was obtained by the corresponding Poisson's ratio ranging from 61.39 kPa to 66.30 kPa. The percentage errors of the estimated Young's modulus in comparison with the assigned Young's modulus (E = 60 kPa) of FE simulation ranged from 2.31 % to 10.51 %.

Table 7 Comparison between estimated results of Young's modulus (in kPa) using estimated Poisson's ratios and the assigned value used in FE simulation (indentor radius = 4.5 mm, Young's modulus = 60 kPa and Poisson's ratio = 0.45).

	***a/h* = 0.6**	**0.8**	**1.0**	**1.5**	**2.0**
2.5%/0.1%	63.24	65.68	62.44	61.49	62.74
5.0%/0.1%	65.19	66.25	62.95	61.45	62.11
10.0%/0.1%	66.45	66.97	62.23	61.22	61.77
Average	64.96	66.30	62.54	61.39	62.20
Percentage error	8.26%	10.51%	4.23%	2.31%	3.67%

3.3.3 Summary

The results of FE analysis demonstrated that simultaneous estimation of Poisson's ratio and Young's modulus in single-indentation could be realized by using the ratio between two kappa values with two different deformation ratios. From Table 6, it was noted that the percentage errors were limited within – 2.0 % when the aspect ratio was equal to or larger than 1.0. As the Young's modulus was estimated using the estimated Poisson's ratio, the percentage errors of estimated Young's modulus could be greatly reduced below 5.0 % when the aspect ratio was or greater than 1.0. Similar to the FE simulation studying the effects of finite deformation on double-indentation with two different sized indentors, better results of estimated Poisson's ratio could be obtained when the aspect ratio was between 1.0 to 2.0. It might be due to the larger substrate effects found in the thin tissue, which cannot be totally reflected by the kappa factor.

3.4 Estimation of Young's Modulus and Poisson's Ratio by Single-Indentation using Deformation Dependent Indentation Stiffness

3.4.1 Methods

The FE models used to study single-indentation using the deformation-dependent indentation stiffness were the same as described in section 4.3.1. The radius of the indentor was set to be 4.5mm. The thickness of the soft tissue in the FE model was changed in order to build the FE models with different aspect ratios a/h (0.6, 0.8. 1.0, 1.5 and 2.0). The assigned Poisson's ratio and Young's modulus was 0.45 and 60kPa, respectively. The Poisson's ratio and Young's modulus were estimated using equation (25) and (26). To demonstrate the effect of the total deformation on the result of estimation, indentation data within deformation ratios of

1%, 2.5% 5% and 10% were used to obtain corresponding Poisson's ratio and Young's modulus.

3.4.2 Results

Figure 21 illustrated that the force - deformation curve obtained from the FE simulation (aspect ratio = 2.0, Young's modulus = 60 kPa and Poisson's ratio = 0.45). The nonlinear effect could be observed more obviously when the deformation ratio is more than 10%. This nonlinearity is proposed to be caused by the substrate effect of tissue, which is related to the Poisson's ratio. The deformation-dependent indentation stiffness can be obtained based on equation (24) (Figure 22). The y-axis and x-axis of the graph are the indentation stiffness P/w and deformation ratio w/h, respectively. In Figure 23, β was found to be 1.23 N/mm which is the result of y-intercept, 4.38N/mm, divided by the value of slope, 2.45 and it can be used to calculate the Poisson's ratio using the relationship between the β and Poisson's ratio found in Table 1.

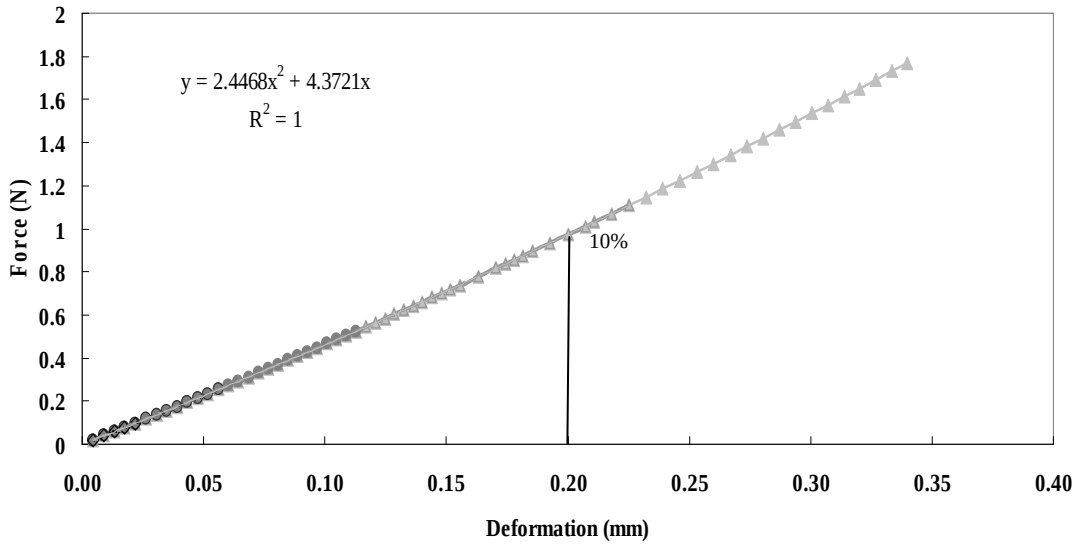

Figure 21 Force - deformation data obtained using the FE simulation for indentation with aspect ratio being 2.0, indentor radius 4.5 mm, Young's modulus being 60 kPa and Poisson's ratio 0.45. The force - deformation curve includes slight nonlinearity slightly and it could be fitted by a quadric function.

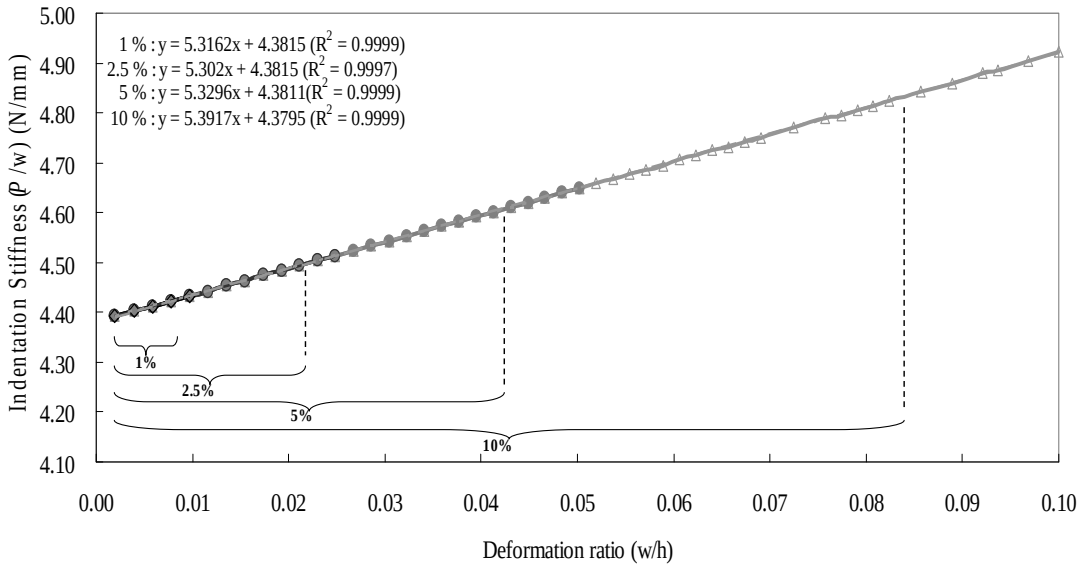

Figure 22 The relationship between the indentation stiffness (*P*/*w*) and deformation ratio (*w*/*h*) extracted from the indentation data in Figure 21. Different colour lines (red, blue, yellow and purple) indicated different deformations of the indentation stiffness (1%, 2.5%, 5% and 10%). Equations were shown for the values of slope and y-intercepts for the force - deformation curve with various deformation ratios.

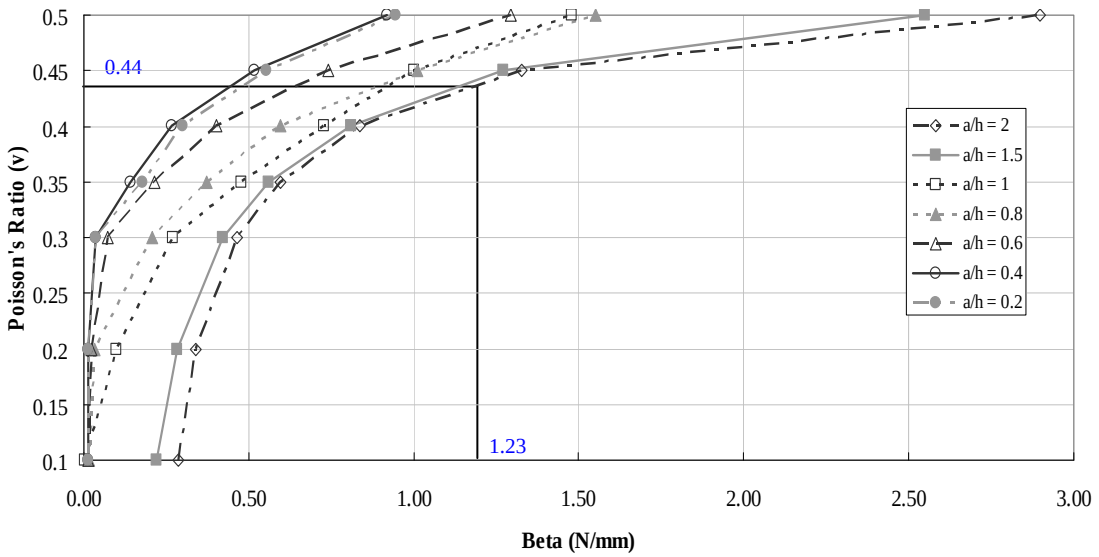

Figure 23 The relationships between factor β and Poisson's ratio for different aspect ratios (from 0.2 to 2.0). The previous β factor (1.23N/mm) was used to estimate the Poisson's ratio and the result was 0.44. The assigned values of Young's modulus, Poisson's ratio and aspect ratio of this FE model were 60kPa, 0.45 and 2.0 (the dotted line with hollow diamond at the most right hand side), respectively.

By using interpolation, Poisson's ratio could be obtained using the known data points of the relationship between β and Poisson's ratio. Table 8 showed the results of simultaneously estimated Poisson's ratio and Young's modulus using single-indentation. In this table, Young's modulus and Poisson's ratio were estimated by force - deformation data under different deformation ratios (1%, 2.5%, 5% and 10%) together with the percentage differences in comparison with the assigned Young's modulus and Poisson's ratio in FE simulation (E = 60 kPa and v = 0.45). From Table 8, the errors of the estimated Poisson's ratio ranged from -1.7% to -8.2% when the aspect ratio ranged from 0.6 to 2.0. For the Young's modulus, the estimation errors of the estimated values ranged from +3.0% to +9.1% when the aspect ratio was between 0.6 and 2.0.

Table 8 The Poisson's ratio and Young's modulus extracted from the simulated indentation data by single-indentation with various aspect ratios (from 0.6 to 2.0) and deformations ratios (from 1% to 10%). The percentage errors indicated the difference between the estimated and assigned values of the parameters. (E = 60 kPa and v = 0.45).

w/h	**Poisson's ratio & Young's modulus**	**Aspect ratio *a/h***					**mean**	**% error**
		0.6	**0.8**	**1.0**	**1.5**	**2.0**		
0.1	***v***	0.413	0.420	0.438	0.438	0.440	0.430	-4.5 %
	% error	-8.2 %	-6.7 %	-2.6 %	-2.8 %	-2.2 %		
	E	65.4	65.3	62.6	63. 7	63.7	64.1	6. 9 %
	% error	9.1%	8.9%	4.3 %	6.1 %	6.1 %		
0.05	***v***	0.423	0.423	0.440	0.436	0.439	0.432	-4.00 %
	% error	-5.9 %	-6.0 %	-2.3 %	-3.0 %	-2.5 %		
	E	63.9	64.7	62.3	64.0	64.1	63.8	6.34 %
	% error	6.5 %	7.9 %	3.8 %	6.6 %	6.9 %		
0.025	***v***	0.429	0.425	0.441	0.436	0.438	0.435	-3.2 %
	% error	-4.8 %	-5.5 %	-2.1 %	-3.2 %	-2.7 %		
	E	63.1	64.3	62.1	64.2	64.3	63.6	6.0 %
	% error	5.2 %	7.2 %	3.5 %	7.0 %	7.2 %		
0.01	***v***	0.424	0.426	0.442	0.436	0.438	0.433	-3.7 %
	% error	-5.8 %	-5.4 %	-1.7 %	-3.1 %	-2.6 %		
	E	63.8	64.3	61.8	64.1	64.2	63.6	6.0 %
	% error	6.3 %	7.1 %	3.0 %	6.8 %	7.1 %		
	***v* mean**	0.422	0.424	0.440	0.437	0.439		
	***v* % error**	-6.2 %	-5.9 %	-2.2 %	-3.0 %	-2.5 %		
	***E* mean**	64.1	64.7	62.2	64.0	64.1		
	***E* % error**	6.8 %	7.8 %	3.7 %	6.6 %	6.8 %		

3.4.3 Summary

From the results of FE simulation, simultaneous estimation of Poisson's ratio and Young's modulus in single-indentation was feasible to be applied using the force - deformation. According to the results in Table 8, the optimized aspect ratio for indentation was between 1.0 and 2.0. It may be due to the fact that thin tissue more obvious deformation-dependent exhibited higher substrate effects. Therefore, the proposed method might be suitable for the estimation of soft thin tissue or used with larger indentor.

3.5 Overall summary from FE analysis

According to the FE results, it was revealed that double-indentation using two different sized indentors with considering finite-deformation, as well as single-indentation with different deformation ratios and the deformation-dependent indentation stiffness were feasible to estimate the Poisson's ratio. With the known Poisson's ratio, the accuracy of estimating Young's modulus could be improved. The proposed three methods would be further tested on the phantoms and ArtC for the validation of its feasibility to apply for the *in-vivo* characterization of the mechanical properties of the biological soft tissue.

In clinical application, handheld indentor is always used for testing tissue properties. As aforementioned, the size of indentor is smaller than that of specimen. Therefore, indentation is more feasible to be carried out *in-vivo*. However, *in-vivo* indentation may cause some drawbacks in double-indentation. Firstly, the alignment of the handheld indentor may be changed between two indentations which may contribute to inconsistent and inaccurate result. Secondly, relaxation time should be provided between two indentations in order to ensure that the tissue can recover to its

original condition. And ions and fluid flow may happen at anytime in various patterns in biological tissues. As, the effects of those biological changes on mechanical properties are still unknown, using single-indentation may help to reduce the experimental errors compared with double-indentation.

Chapter 4 Experimental Study on Phantoms

Two different kinds of silicone phantoms were prepared for the experimental validation for the proposed methods. By comparing the Poisson's ratio and Young's modulus of the silicone phantoms, measured by the unconfined compression and indentation with the proposed calculation algorithms, the feasibility of applying the algorithms for tissue mechanical properties test could be validated. In this chapter, the procedures of preparing and indenting different silicone phantoms together with the steps of calculation using the proposed algorithms are first presented. The discussion is then given based on the results of this experimental study on silicone phantoms.

4.1 Preparation for Silicone Phantoms

In this study, the silicone phantoms used for the experiment were assumed to be homogenous, isotropic and linearly elastic. As the features and the fabricating procedures of materials would affect the mechanical testing results of silicone phantoms, it was important that the preparation procedures should be kept constant. In this study, the silicone phantoms which were used for the experiment were fabricated by ourselves and an external collaborator.

4.1.1 Fabrication of Silicone Phantoms

Two shapes of silicone phantom specimens were prepared (Figure 24) by using liquefied silicone with 10% of condensing catalyst (Wacker M4648, Wacker Chemicals Hong Kong Ltd., HK, China), including thin circular sheet with different thicknesses and a cubic shaped specimen. Three numbers of thin circular sheets with two different thicknesses were prepared for the indentation test. After interfusing catalyst into liquefied silicone in container, the mixture was slowly stirred to ensure even and complete mixing between the catalyst and silicone for chemical reaction. After stirring, the container was put in a steady place for 5 minutes in order to release the air bubbles inside the liquefied silicone-catalyst mixture. The condensation reaction could be indicated by the exothermal reaction. After filling the liquefied mixture into molds (Figure 25), the molds with mixture were put under room temperature (~25 ℃) for at least 24 hours for complete condensation. The mixture was placed into the vacuum pump container in order to release the bubbles in the phantoms.

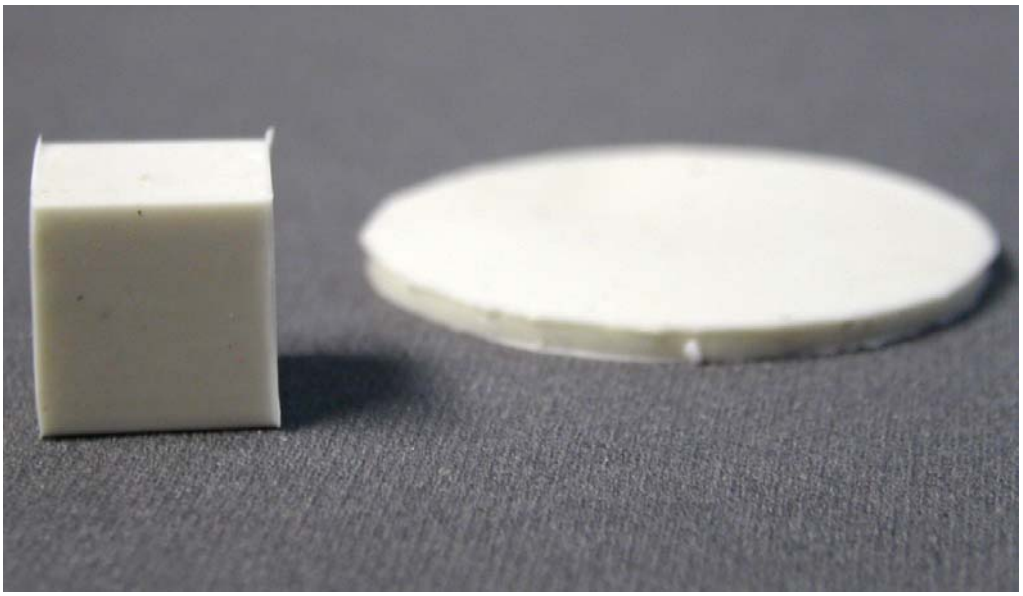

Figure 24 Two different shapes of silicone phantoms. The right one is the thin circular sheet and the left one is the cubic specimen.

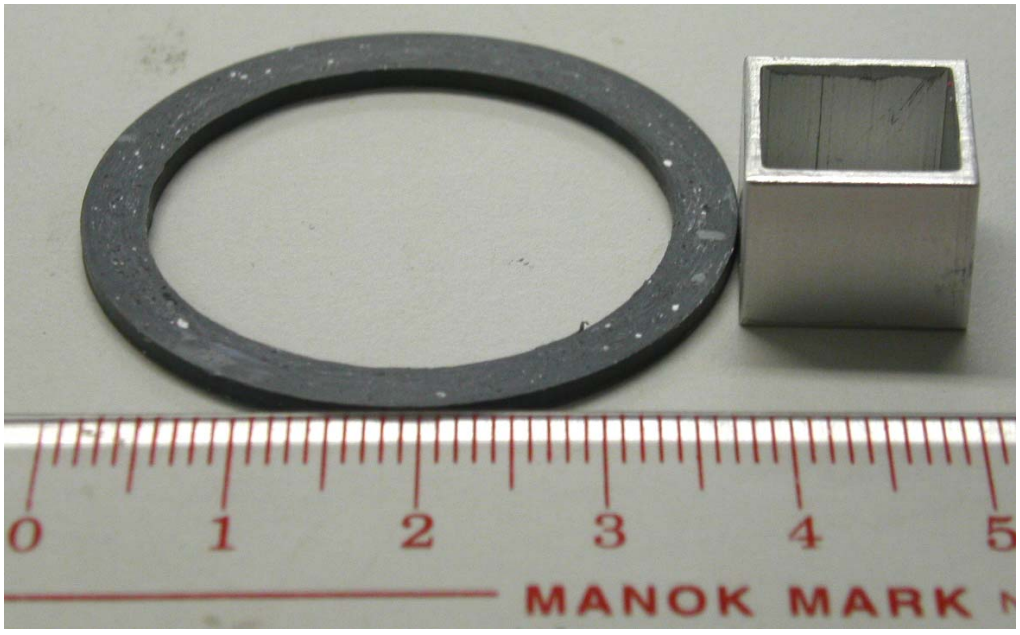

Figure 25 Two different shapes of molds were applied to prepare different types of silicone phantom. The left one was used for fabricating circular sheet phantom and the right one was for making the cubic phantom.

4.1.2 Silicone Phantoms from External Collaborator

By collaborating with Centre of Mechanics of ETH Zurich in Switzerland, we had another set of silicone phantoms which had been studied earlier (Hollenstein, 2005). The aim of that previous study was to compare different kinds of material testing methods. Its results could be applied for validating the proposed calculation algorithms. The silicone phantoms prepared for this study used the same materials as Truth Cube 2 (TC-2), which was made from platinum-catalyzed silicone rubber material (Ecoflex 0030, Smooth-On Inc., PA, US) (Figure26) and had been tested by uniaxial unconfined compression together with other custom-made methods, such as tissue aspiration, torsional resonator device and tissue material property sampling tool tests (Hollenstein *et al.,* 2006), and the mechanical properties of TC-2 had been determined.

Several circular sheet phantoms with the same material and fabrication protocol as TC-2 silicone phantoms were prepared for this experiment (Figure 27). The Young's modulus and Poisson's ratio of the TC-2 material obtained by uniaxial unconfined compression was approximately 29.45 kPa and 0.5, respectively. The mass density of the TC-2 material was approximately 1070 kg/m^3.

Figure 26 The cylindrical silicone phantom called Truth Cube 2 (TC-2). Both the diameter and height of this phantom are approximately 82.5mm (Hollenstein, 2005).

Figure 27 Three circular sheet silicone phantoms were fabricated from a material with almost the same mechanical properties as TC-2 silicone phantom, which was prepared for indentation test in this study.

4.2 Uniaxial Compression tests for Reference Phantoms

Although the thickness values of both TC-2 and Wacker silicone phantoms were assigned before production, the actual thickness of various silicone phantoms would still differ from the assigned value due to the experimental errors during fabrication. Therefore, their thickness was measured during the test, Instron MTM was used for thickness measurement by its Linear Variable Differential Transformer (LVDT) together with the load cell, which would determine the initial contact between indentor and surface of phantom by measuring the significant changes of the reaction force (Figure 28). Afterwards, phantom was removed from the flat plane and indentor was applied again on the surface (Figure 29). The displacement of the indentor was measured by LVDT, which is the thickness of phantom. The initial force was assigned at 0.05 N driven by MTM program. Table 9 showed the summary of mechanical properties and thickness values of the silicone phantoms, including TC-2 and Wacker.

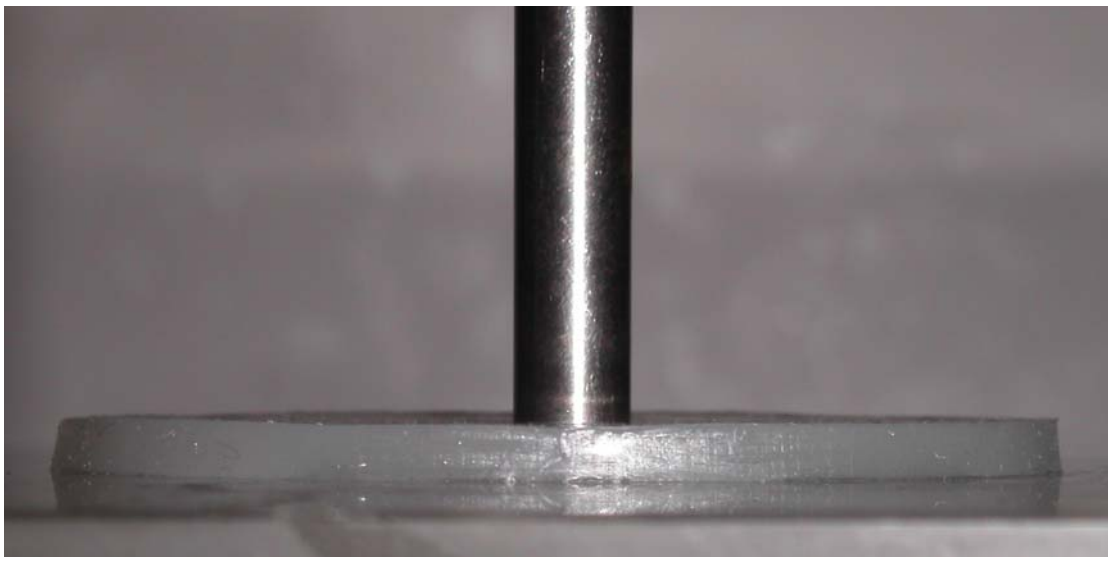

Figure 28 The moment of indentor touched the surface of silicone phantom. It was determined by load cell (Force > 0.05 N).

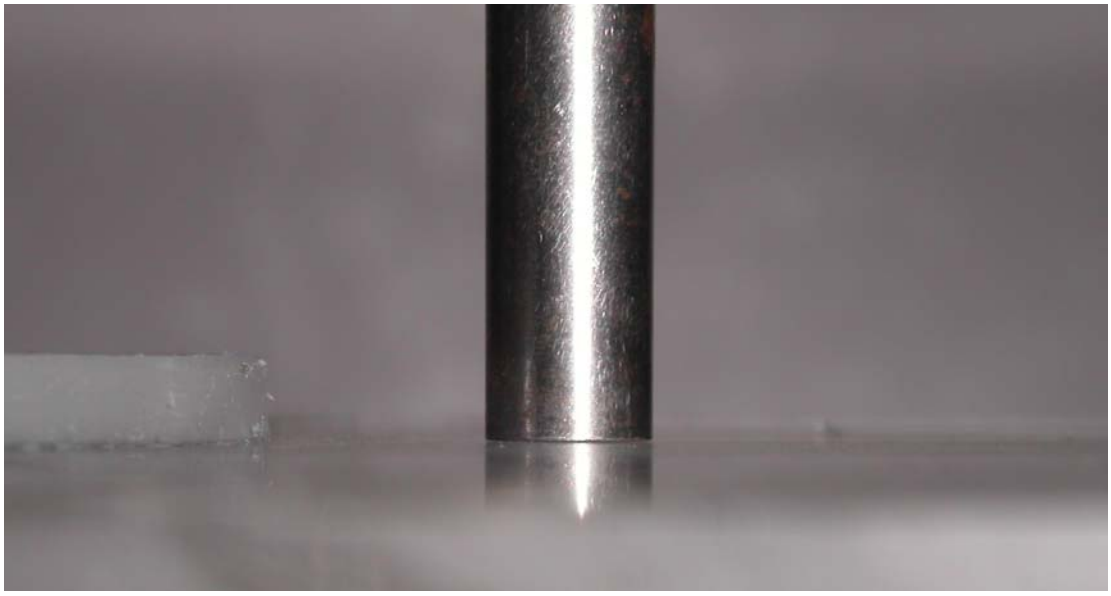

Figure 29 The moment of indentor touched the surface of flat plane. The displacement of indentor was measured by LVDT as the thickness of the silicone phantom.

Table 9 Summary of the mechanical properties of silicone phantoms.

Parameters	**TC – 2 Phantoms (Phantom A)**			**Wacker Phantoms (Phantom B)**		
Young's modulus	29.4kPa			200kPa		
Poisson's ratio	0.50			0.37		
Diameter	25mm			25mm		
Phantom and corresponding Thickness	1A 1.56mm	1B 1.64mm	1C 1.52mm	2A 2.40mm	2B 2.47mm	2C 2.74mm

Phantom thickness could be effectively measured by this method. 0.05 N preload was assigned to indicate the initial contact between the indentor and surface of silicone phantom. However, if the surface of silicone phantom is not smooth and flat enough, measurement errors may be caused The effects will be further discussed later.

4.3 Indentation tests on Phantoms

After preparing silicone phantom, indentation experiment was carried out using the material testing system. For Phantom A (Table 9), the results were used to validate the feasibility of estimating Poisson's ratio and Young's modulus by single-indentation with deformation dependent indentation stiffness, single-indentation with two different deformations and double-indentation with two different sized indentors as the mechanical properties of Phantom A had been tested and determined previously in the former study.

For Phantom B (Table 9), the Poisson's ratio and Young's modulus were estimated by the mechanical testing machine with the method of single-indentation with deformation dependant indentation stiffness, single-indentation with two different deformations and double-indentation using two different sized indentors.

After preparing the silicone phantoms for testing, the material testing system (MTM) was used for the indentation test. In this study, a desktop testing system (Instron Series 5560, Instron Corporation, MA, US) with 10 kN load cell (model 5569) was employed (Figure 30). Two indentors with different radius (1.5 mm and 3.0 mm) were used for the indentation test on silicone phantoms as shown in Figure 31.

Figure 30 Instron material testing machine (Model 5569, Instron Series 5560, Instron Corporation, MA, US).

Figure 31 Indentors with different radius (from left to right, 1 mm, 1.5 mm, 2 mm and 3 mm).

Each circular sheet of silicone phantom was visually aligned with the indentor at the centre of the phantom on a flat plane. Then, lubrication oil was applied on the surface of silicone phantom to avoid the friction between the interface of silicone phantom surface and indentor (Hayes *et al.*, 1972; Zhang *et al.*, 1997). The indentation rate was set to be 1.5 mm/s (Jin and Lewis, 2004) and every phantom was indented for 3 times. Five minutes was given for recovering between each indentation. Both Phantoms A and B were tested using Instron MTM with the above protocol (Figure 32).

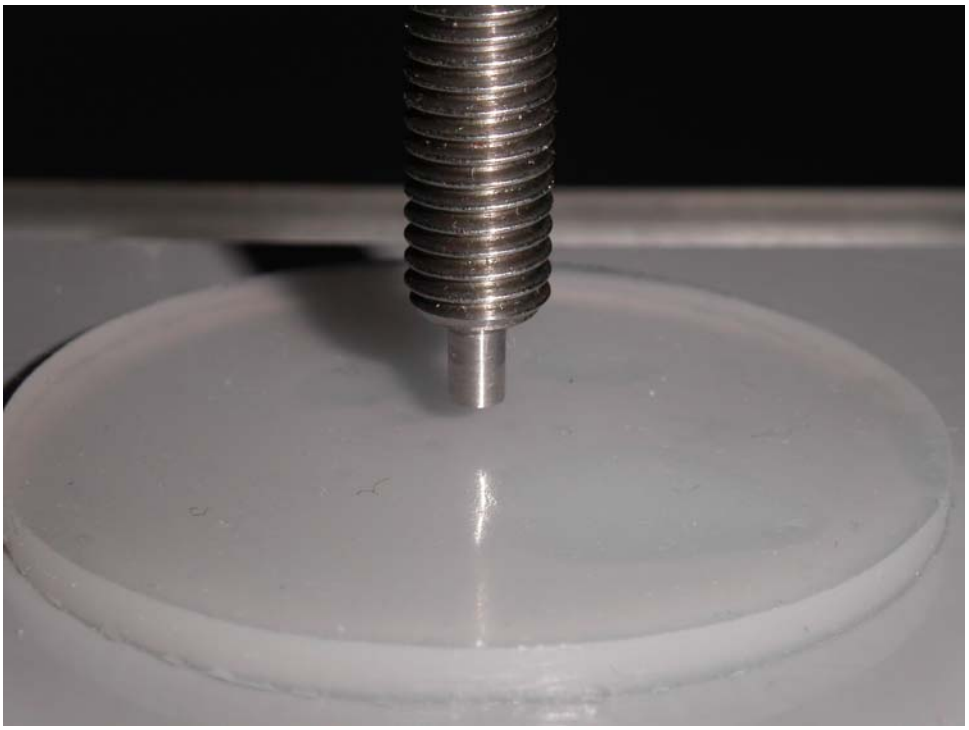

Figure 32 Indentation on the silicone phantom using Instron material testing system, indentor radius was 1.5 mm.

4.4 Results

Two different types of silicone phantoms underwent different combinations of indentation and proposed calculation algorithms. For Phantom A, indentations using Instron MTM were carried out. The force and deformation data were extracted to estimate Poisson's ratio and Young's modulus by double-indentation with two different sized indentors and also by single-indentation with deformation-dependent indentation stiffness.

For Phantom B, the phantoms were tested by MTM. The data were analyzed by double-indentation with two different sized indentors and single-indentation with two different deformations. The results were compared with those obtained by the single-indentation with deformation dependent indentation stiffness using Instron MTM.

4.4.1 Results of Phantom A

Table 10 shows the Poisson's ratio and Young's modulus of Phantom A estimated by two different calculation algorithms. For the data measured by single-indentation with deformation-dependent indentation stiffness (2a & 2b), the average Poisson's ratio and Young's modulus of all specimens was estimated as 0.45 and 19.79 kPa, respectively. For the data measured double-indentation with two different sized

indentors (3a & 3b), the average Poisson's ratio and Young's modulus for all specimens was 0.48 and 22.2 kPa, respectively. For the data measured by single-indentation with two different deformations (4a & 4b), the average Poisson's ratio and Young's modulus of all specimens was estimated as 0.40 and 28.76 kPa, respectively.

In comparison with the values measured by unconfined compression in a pervious study (Hollenstein M., 2005), the percentage differences of Poisson's ratio and Young's modulus ranged from -2 % ~ -28 % and +42 % ~ -4.6 %, respectively.

Table 10 The reported values (Hollenstein M., 2005) and estimated values of Poisson's ratio and Young's modulus which were obtained by Instron MTM with 2 different calculation algorithms (using deformation-dependent indentation stiffness and ratio of two kappa values with two different sized indentors) (TC-2 phantom).

Mechanical Properties measured by different methods		**TC-2 silicone phantom specimens**		
		A	**B**	**C**
Reported Value obtained by unconfined compression	1a. Poisson's ratio	---------- ~ 0.5 ----------		
	1b. *E* modulus (kPa)	---------- ~ 29.45 ----------		
Single-indentation with Deformation-dependent indentation stiffness	2a. Poisson's ratio	0.46	0.46	0.44
	Mean of Poisson's ratio		0.45	
	2b. *E* modulus (kPa)	21.41	17.20	20.77
	Mean of *E* modulus (kPa)		19.79	
Double-indentation with Two different sized indentors	3a. Poisson's ratio	0.48	0.49	0.47
	Mean of Poisson's ratio		0.48	
	3b. *E* modulus (kPa)	21.49	19.81	25.58
	Mean of *E* modulus (kPa)		22.29	
Kappa ratio with two different deformations	4a. Poisson's ratio	0.36	0.44	0.39
	Mean of Poisson's ratio		0.40	
	4b. *E* modulus (kPa)	29.36	30.82	26.11
	Mean of *E* modulus (kPa)		28.76	

4.4.2 Results of Phantom B

Similar to the experimental study on Phantom A, force-deformation data of Phantom B was also obtained by Instron MTM with the calculation algorithm of single-indentation with deformation-dependent indentation stiffness. Besides, TUPS with two different sized US probes was used to carry out indentation test on Phantom B. Both ratios between two kappa values with different sized indentors and different deformations were used to estimate the Poisson's ratio and Young's modulus. The results were shown in Table 11.

For the data measured by single-indentation with deformation-dependent indentation stiffness (2a & 2b), the average Poisson's ratio and Young's modulus of all specimens was estimated to be 0.38 and 218 kPa, respectively. For the data measured by double-indentation with two different sized indentors (3a & 3b), the average Poisson's ratio and Young's modulus of all specimens was estimated to be 0.40 and 193 kPa, respectively. For the data measured by single-indentation with two different deformations (4a & 4b), the average Poisson's ratio and Young's modulus of all specimens was estimated as 0.37 and 234.84 kPa, respectively.

Table 11 The original values and estimated values of Poisson's ratio and Young's modulus which were obtained by Instron MTM with 3 different algorithms (using deformation-dependent indentation stiffness, ratio of two kappa values with two different sized indentors and ratio of two kappa values with different deformations) (Wacker phantom).

Mechanical Properties measured by different methods		**Wacker phantom specimens**		
		A	**B**	**C**
Original values (by unconfined compression)	1a. Poisson's ratio	---------- ~ 0.37 ----------		
	1b. *E* modulus (kPa)	---------- ~ 200.00 ----------		
Deformation-dependent indentation stiffness	2a. Poisson's ratio	0.38	0.38	0.38
	Mean of Poisson's ratio		0.38	
	2b. *E* modulus (kPa)	227.56	218.89	210.40
	Mean of *E* modulus (kPa)		218.95	
Kappa ratio with two different sized indentors	3a. Poisson's ratio	0.41	0.39	0.41
	Mean of Poisson's ratio		0.40	
	3b. *E* modulus (kPa)	195.66	191.20	194.48
	Mean of *E* modulus (kPa)		193.78	
Kappa ratio with two different deformations	4a. Poisson's ratio	0.35	0.33	0.42
	Mean of Poisson's ratio		0.37	
	4b. *E* modulus (kPa)	243.77	246.84	213.92
	Mean of *E* modulus (kPa)		234.84	

In comparison with original values measured by unconfined compression (1a and 1b) in Table 11, the percentage differences of Poisson's ratio and Young's modulus ranged from -13.5 % ~ +10.8 % and -23.42 % ~ +4.4 %, respectively. Comparisons between the estimated values measured by Instron MTM (2a and 2b) with the calculation algorithm by single-indentation with deformation-dependent indentation

stiffness and the estimated values measured by TUPS with the algorithms using kappa ratios with two different sized indentors and two different deformations were carried out. The results were shown in Table 12.

Table 12 The percentage differences of the mean values of Young's modulus and Poisson's ratio between different calculation algorithms (Wacker phantom).

Combinations of comparisons of different calculation algorithms	**Percentage change of *E* modulus**	**Percentage change of Poisson's ratio**
Instron with Deformation-dependent indentation stiffness vs. Kappa ratio with two different sized indentors	+11.5%	-5.2%
Instron with Deformation-dependent indentation stiffness vs. Kappa ratio with two different deformations	-7.26%	+2.6%

4.5 Summary

Two types of silicone phantom were tested, including TC-2 (Phantom A) and Wacker (Phantom B) silicone phantoms. The major difference between TC-2 and Wacker silicone phantoms was found in their Young's moduli using unconfined compression test, the reference Young's modulus of TC-2 and Wacker silicone phantoms was measured as 29.4 kPa and 200 kPa, respectively. Therefore, the Young's modulus of Wacker is nearly 5.8 times more than that of the TC-2 silicone phantom. According to the results shown in tables 10 and 11, the results showed that

the percentage differences of the estimated Poisson's ratio of both phantoms were less than 10 % in comparison with their corresponding reference values. However, the percentage differences of estimated Young's modulus of Wacker phantom were much smaller compared with the TC-2 phantom, in comparison with their corresponding reference values. The reasons for the relatively large percentage differences of the estimated Young's moduli might be due to the experimental setup and the variation of the procedures of the phantom preparation for the reference specimens (uniaxial compression tests) and the test specimens (indentation tests).

In the procedures of preparing silicone phantoms, molds were used to ensure the shape of circular sheet phantom (Figure 25). Using this method, the smoothness of the border and bottom surface of the circular flat sheet can be ensured. However, the smoothness of top surface can only rely on the gravity and the diffusion of liquefied silicone-catalyst mixture. Thus the phantoms surface might not be perfectly flat and smooth.

For both unconfined compression and indentation, 10 % deformation control was set. As the surface area of compressor was larger than that of phantom specimen, it could cover the whole surface of phantom during unconfined compression. Therefore, the effects of uneven and relatively rough top surface on unconfirmed compression test were relatively lesser than those in indentation. Furthermore, if small

bubbles were formed in silicone phantom during fabrication, it may further affect the results of indentation. The method of improvement is to apply more effective vacuum pump during the procedure of fabricating of silicone phantoms to remove all potential bubbles and flatten the top surface by the evenly distributed air pressure. The volume of catalyst can be reduced to slow down the condensation reaction in order to provide sufficient time for the action of gravity to have a smooth top surface.

In summary, the algorithms could be applied to estimate the mechanical properties of the silicone phantoms, especially the Poisson’s ratio. The differences between the reference values and the estimated values can be minimized by applying more powerful vacuum pump and a smaller potion of catalyst in the procedures of phantom fabrication.

Chapter 5 Experimental Study on Articular Cartilage

After the experimental study on silicone phantom to test the feasibility of using the proposed methods for assessing the mechanical properties of soft tissues, further experiment was also carried out on ArtC of bovine patellae for demonstration of the practical application of those proposed calculation algorithms. By applying the calculation algorithms, mechanical properties of the bovine patella ArtC were estimated and compared. Moreover, the indentation was also carried out before and after trypsin enzyme digestion for simulating the situation of osteoarthritis, i.e. the degeneration of articular caused by injury, aging, repeating loading, genetic defects or pathological changes. The articular cartilage tended to be softer after trypsin digestion as the content of (Proteoglycans) PGs in ArtC was largely reduced (Mow and Ratcliffe, 1997).

5. 1 Specimen Preparation

Fresh bovine patellae (Figure 33) without any observable damage on the cartilage surface were bought from wet market. Isotonic phosphate buffered saline (PBS) solution (0.15M NaCl) was applied to rinse the ArtC surface. Then, the ArtC surface was covered by bandage with isotonic PBS solution for preventing the dehydration of

ArtC. A fixing device was used to mount the patella on the 3 way camera head platform (Figure 34) to the Instron MTM. A 3D ball head platform was used for adjusting the orientation of the whole bovine patella in order to ensure the indentor could align with the axial axis and be perpendicular to the ArtC surface. As the minimum distance between fixing device and indentation site was at least 5 times larger than the radius (> 15mm), therefore the force generated by fixing device, as a part of boundary condition could be ignored (Spilker *et al*., 1992).

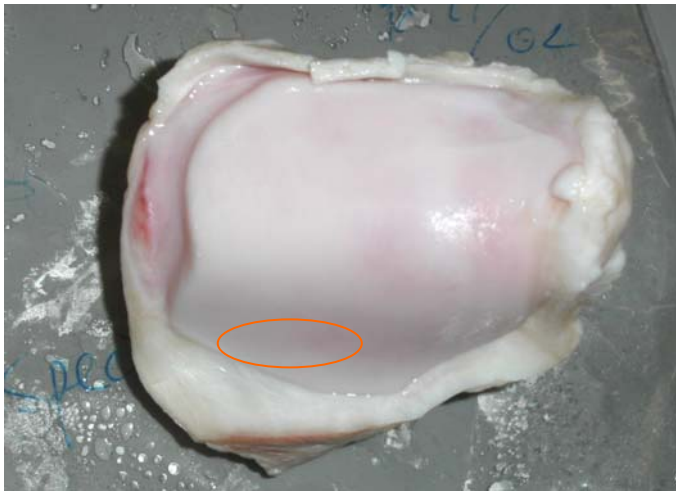

Figure 33 Fresh bovine patella with a layer of articular cartilage was bought from market and rinsed by isotonic PBS solution before experiment. The orange circle indicates the tested flat area located at the lateral articular facet of the patella.

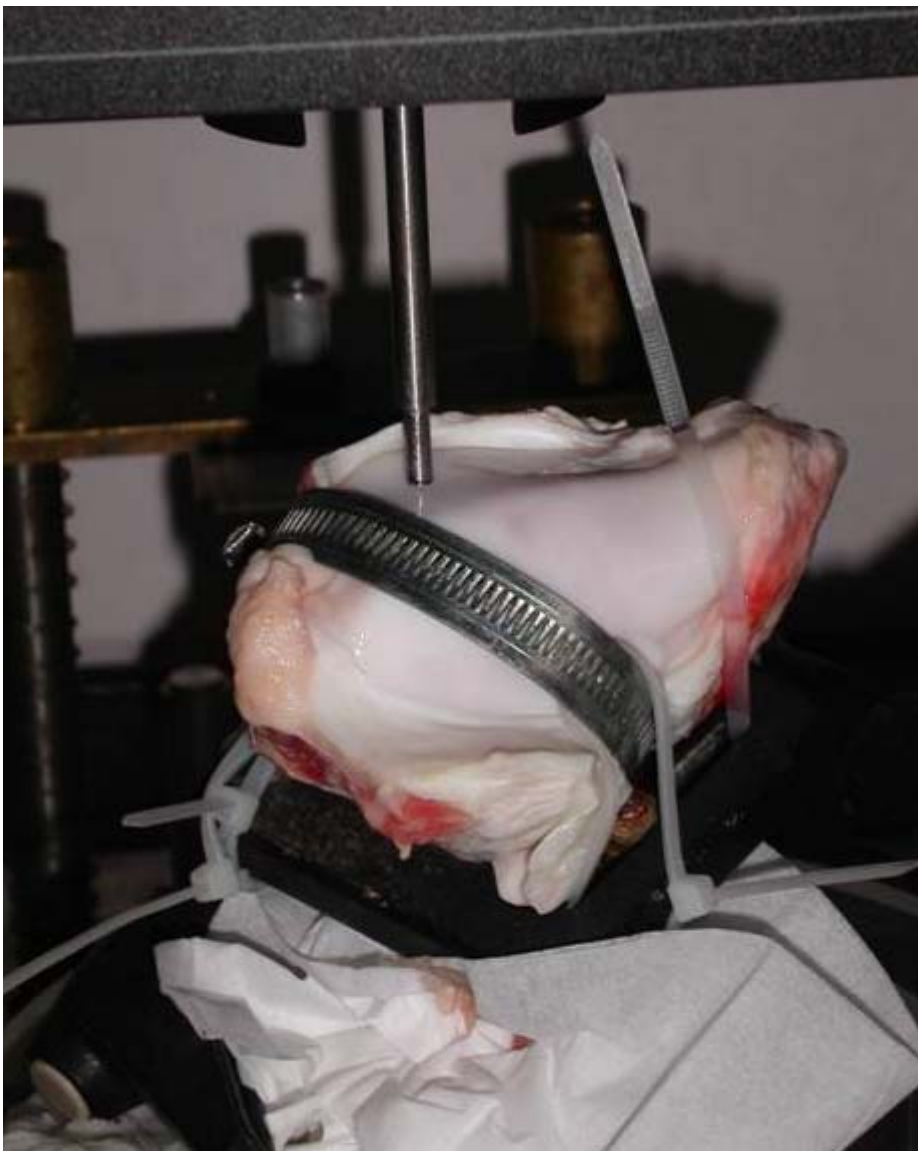

Figure 34 Experimental setup of the indentation for ArtC. The ArtC was mounted on the 3D ball head platform by the metallic fixing device. Other plastic wire ropes were also applied to further enhance the fixation of the setup.

During the whole period of experiment, bandage with isotonic PBS solution was applied to cover and submerge the whole surface of ArtC to prevent any dehydration when the ArtC was not being indented. Isotonic PBS solution was added to the bandage by a dropper every 15 minutes. Room temperature and humidity was kept in constant (22℃ ± 1℃, RH 70% ± 2%) throughout the experiment to eliminate the effects of changes of environmental factors. Totally four bovine patella were tested in this experiment.

5.2 Enzyme Digestion of Articular Cartilage

After normal indentation, the ArtC surface of patella was rinsed by isotonic PBS solution and completely submerged into trypsin enzyme solution for 4 hours in an incubator at 37℃. Trypsin enzyme solution (0.25% trypsin solution, GiBco, Canada) without any further dilution was used to decompose the PGs in the cartilage and would cause the reduction of the compressive modulus of ArtC. According to the results reported in an early study, the PGs could be 82.3 ± 20.3 % removed after such trypsin treatment (Moody *et al.*, 2006).

After digestion by trypsin enzyme, the whole patella was taken out and rinsed completely by isotonic PBS solution. Afterwards, the same mechanical indentation was carried out as on normal cartilage to collect the force-deformation data for

estimating the changes of mechanical properties.

5.3 Experiment on Articular Cartilage

5.3.1 Thickness Measurement

In this study, needle punching technique was applied to measure the tissue thickness of ArtC (Swann and Seedhom, 1989). Four specimens were chosen. After the specimen was fixed on the 3D ball head platform, a needle indentor was applied to punch into the ArtC of bovine patella, and the changes of the punching force were recorded by MTM. The sudden changes in the force as shown in Figure (36) were recorded and used as indicators for different moments.

The thickness of ArtC could be estimated by the displacement during the time period when the needle just penetrated the surface and when the needle penetrated into the underlying bone of ArtC (Figure 36). Five points were selected near the indentation site which was the flat area of lateral articular facet of the bovine patella (Figure 33). The average values of tissue thickness of four bovine ArtC samples were shown in Table 13.

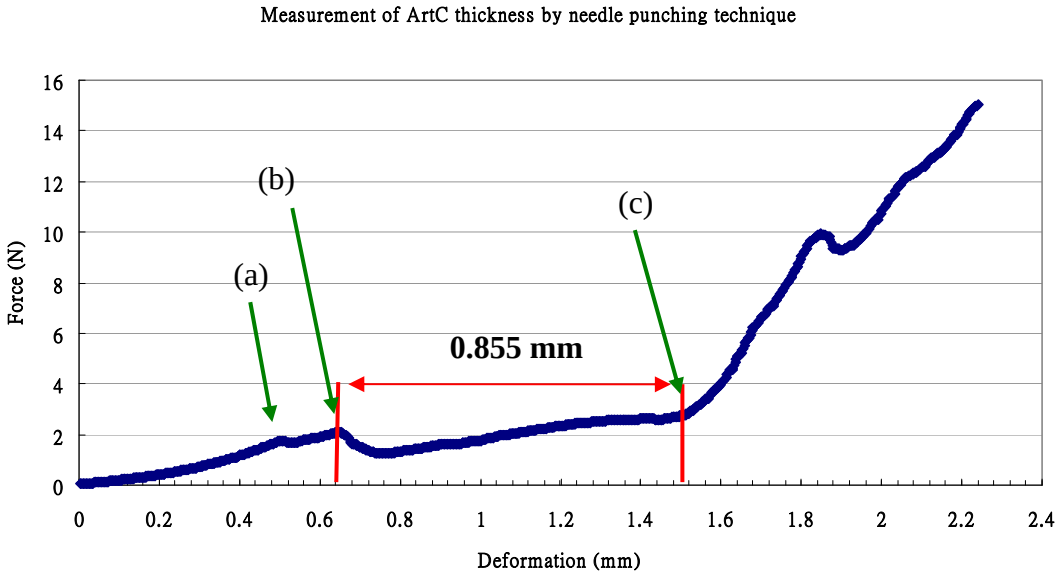

Figure 35 Force-deformation curve obtained by needle indentor. Tissue thickness can be measured by the changes of force applied (due to tissue stiffness) on the tissue. In this example, the thickness of the ArtC sample is 0.855 mm. (a) the tip of needle touches the surface of ArtC, (b) the needle totally penetrate the surface of ArtC and (c) the needle touches and starts to penetrate the underlying bone of ArtC

Table 13 Means of the tissue thickness around indentation location of four bovine ArtC specimens.

	Bovine ArtC specimens			
Thickness (mm)	**A**	**B**	**C**	**D**
Location 1	0.83	0.77	0.63	0.88
Location 2	0.76	0.68	0.61	0.86
Location 3	0.72	0.66	0.59	0.82
Location 4	0.62	0.63	0.59	0.76
Location 5	0.66	0.66	0.62	0.68
Average tissue thickness (mm)	0.72	0.68	0.61	0.80

The range of average thickness of the ArtC layer from four bovine patellae was found between 0.61 mm and 0.80 mm. The mean of thickness was found approximately 0.70 mm. The average tissue thickness of each specimen (Table 13) was further used for the estimation of Poisson's ratio and Young's modulus.

5.3.2 Indentation Tests and Analysis

After measuring the thickness of ArtC, mechanical indentations were carried out for estimating the mechanical properties of ArtC. The experimental setup of the mechanical indentation was similar to the previous setup for thickness measurement, but a flat-ended cylindrical indentor was applied instead of the needle indentor (Figure 31). The whole bovine patella was fixed on the 3D ball head platform (Figure 35). Flat area on lateral articular facet of bovine patella (Figure 33) was visually chosen for the indentation test. Moreover, the 3D ball head platform was adjusted to ensure the flat area was visually perpendicular to the indentor (Figure 34).

A flat-ended cylindrical indentor with radius of 3 mm was used for mechanical indentation. The indentation rate was set to be 1.5 mm/s (Jin and Lewis, 2004) and the indentation depth was up to 10% of its original thickness of the ArtC layer. Three testing trials were carried out for each patella at the same point. Duration of two hours

was given for the recovery of articular cartilage between two adjacent indentations. During these two hours, the surface of ArtC was covered by bandage with isotonic PBS solution as mentioned earlier to prevent ArtC from rapid dehydration. Besides, the experimental setup, temperature and humidity of environment were kept constant.

Two proposed calculation algorithms were used to calculate the mechanical properties of ArtC layer of bovine patella for comparisons including the algorithms using the deformation-dependent indentation stiffness and the Kappa ratio with two different deformations. The Poisson's ratio and Young's modulus were estimated by these two different algorithms, and results were compared to demonstrate the performances of these proposed algorithms.

5.4 Results

By using the deformation-dependent indentation stiffness and equation (23), the indentation force and deformation were extracted to form a force – deformation (P/w) against deformation ratio (w/h) curve. After linear regression, the slope (m) and y-intercept could be obtained for estimating Poisson's ratio and Young's modulus. The value of slope of the linear equation was used to estimate Poisson's ratio by the β table (Table 1). And, the y-intercept was used to estimate Young's modulus using equation (26). A Matlab program (Matlab 7.0, The Mathworks, Natick, Massachusetts,

US) was applied to carry out interpolation of β table according to the aspect ratio and Poisson's ratio. Table 14 showed the results of Poisson's ratio and Young's modulus, estimated using the algorithm with deformation-dependent indentation stiffness.

Table 14 Summary of the properties of four bovine specimens estimated by the algorithm with deformation-dependent indentation stiffness.

Bovine Specimen	Average Thickness	slope	y-intercept	Beta	Poisson's ratio	Kappa Value	Young's Modulus
		40.5	27.4	1.48	0.462	5.332	2.02 MPa
A		40.8	29.6	1.38	0.458	5.163	2.27 MPa
		39.7	29.8	1.33	0.455	5.09	2.32 MPa
Mean	0.72 mm				0.458		2.21 MPa
		40.2	23.1	1.74	0.470	6.18	1.46 MPa
B		37.5	24.2	1.55	0.462	5.70	1.67 MPa
		52.6	23.2	2.27	0.491	6.94	1.27 MPa
Mean	0.68 mm				0.474		1.46 MPa
		42.7	22.2	1.90	0.473	7.12	1.21 MPa
C		49.2	25.9	1.90	0.473	7.12	1.41 MPa
		49.9	26.8	1.86	0.471	7.03	1.49 MPa
Mean	0.61 mm				0.472		1.37 MPa
		27.2	19.2	1.42	0.454	7.08	1.08 MPa
D		29.8	24.6	1.21	0.439	6.52	1.52 MPa
		36.8	25.2	1.46	0.455	7.18	1.39 MPa
Mean	0.80 mm				0.449		1.33 MPa

Besides, the proposed algorithm of single-indentation with two different deformations was also used to estimate the mechanical properties of patellar ArtC using the force deformation data. Using equations (20 – 22), the Poisson's ratio was estimated by the

ratio between two kappa values with different deformation ratios (5% and 10%). And, the Poisson's ratio was applied to further estimate the Young's modulus by equation (4). Table 15 shows the results of Poisson's ratio and Young's modulus, as estimated by the algorithm of single-indentation with different deformation. Table 16 shows comparison of the results obtained by the two different algorithms.

Table 15 Summary of the properties of four bovine specimens estimated by the single-indentation with two different deformations.

Bovine Specimen	Average Thickness	Ratio between two kappa	Poisson's ratio	Kappa Value	Young's Modulus
		1.059	0.453	4.98	2.37 MPa
A		1.068	0.462	5.34	2.31 MPa
		1.060	0.453	5.01	2.53 MPa
Mean	0.72 mm		0.456		2.40 MPa
		1.090	0.484	6.63	1.48 MPa
B		1.084	0.477	6.34	1.60 MPa
		1.108	0.495	7.08	1.40 MPa
Mean	0.68 mm		0.485		1.50 MPa
		1.077	0.467	6.79	1.42 MPa
C		1.093	0.482	7.66	1.43 MPa
		1.096	0.485	7.83	1.41 MPa
Mean	0.61 mm		0.478		1.42 MPa
		1.099	0.484	8.458	0.88 MPa
D		1.068	0.457	6.821	1.50 MPa
		1.090	0.476	8.001	1.28 MPa
Mean	0.80 mm		0.472		1.39 MPa

Table 16 The comparison of Poisson's ratio and Young's modulus of ArtC of four bovine patelle estimated by two different algorithms.

Bovine Specimen	Mean of Poisson's ratio		Percentage Difference	Mean of Young's modulus (MPa)		Percentage Difference
	Method A	Method B		Method A	Method B	
A	0.458	0.456	0.44 %	2.206	2.402	-8.88 %
B	0.474	0.485	-2.32 %	1.464	1.499	-2.39%
C	0.472	0.478	-1.27 %	1.368	1.419	-3.73%
D	0.449	0.472	-5.12 %	1.330	1.390	-4.51%
Variation of specimens SD %	2.56%	2.62%		25.95%	28.92%	

Besides, Table 17 showed the changes of mechanical properties of ArtC of bovine patella before and after trypsin enzyme digestion. It is obvious that the Young's modulus of ArtC was significantly reduced after trypsin enzyme digestion. The range of Young's modulus of ArtC reduced to the 0.380 MPa ~ 0.993 MPa. The percentage change compared with the Young's modulus before Trypsin enzyme digestion was around -45% to -71%. By the indentation with proposed algorithms, the changes of mechanical properties of ArtC after enzyme digestion can be shown.

Table 17 Table showed the changes of mechanical properties of ArtC of patella.

Bovine Specimen	Young's modulus (MPa)		Percentage Difference
	Specimen without Trypsin digestion	Specimen with Trypsin digestion	
A	2.026 ± 0.16	0.993 ± 0.053	-55.0 %
B	1.464 ± 0.,201	0.806 ± 0.120	-45.0 %
C	1.368 ± 0.142	0.469 ± 0.192	-65.7 %
D	1.330 ± 0.231	0.380 ± 0.217	-71.4 %
Mean	1.592 ± 0.413	0.662 ± 0.287	-59.3 % ± 11.7%

5.5 Summary

The objective of this experimental study is to demonstrate the feasibility of applying those proposed algorithms on ArtC. Thus, the potential of using the algorithms for the measurement of different biological soft tissues could be explored.

Four fresh bovine patellae were tested in the experiment using the algorithm with deformation-dependent indentation stiffness, the Poisson's ratio and Young's modulus ranged from 0.449 - 0.474 and 1.330 MPa - 2.206 MPa, respectively. Using the algorithm of single-indentation with information of different deformations, the Poisson's ratio and Young's modulus ranged from 0.456 ~ 0.485 and 1.390 MPa ~ 2.402 MPa, respectively. As the percentage difference (Table 16) of the results obtained using these two different algorithms were relatively small (< 6% for Poisson's ratio and < 9% for Young's modulus), the results from these two different calculation algorithms were considered to agree with each other. The estimated

Poisson's ratio was equal to or more than 0.449, which might show the instantaneous response of ArtC to the indentation. The tissue fluid in ArtC did not have sufficient time to flow out from ECM. Therefore, the value of Poisson's ratio may represent the total contribution from the liquid phase of tissue fluid and the solid and liquid phases of ArtC. As the indentation rate was same for every indentation test (1.5 mm/s), the instantaneous response might be similar in various ArtC of bovine patella.

However, the variation of Young's modulus of ArtC among these four bovine patellae, was large (>25.95%). It might be due to the variation of different biological tissues and experimental errors. The range of mean of Young's modulus of these four bovine patellar ArtC was from 1.330 MPa ~ 2.206 MPa, which was found to agree with the results in previous studies (Toyras *et al.*, 2001; Chahine *et al.*, 2004).

After trypsin enzyme digestion, single-indentation with the information of deformation-dependent indentation stiffness was carried out on those four bovine patellar ArtC. The Young's modulus was found to be greatly reduced by more than 45.0%. As the stiffness of the articular cartilage became much lower as the collagen-PG solid matrix, which contributes to the largest part of the Young's modulus, was broken down due to the degeneration of PGs by trypsin enzyme digestion. The variation of percentage changes may come from experimental errors and the variation of different biological soft tissues such as composition of collagen –

PG solid matrix and tissue thickness of the ArtC.

The experimental errors may come from the misalignment of the indentor to the surface layer of ArtC. As it was visually and manually adjusted by the 3 way camera head, the surface of ArtC may also not be flat for flat-ended indentation. Moreover, the interface between ArtC and underlying bond may not be flat. These two factors may contribute to the uneven distribution of the indentation force at the indentation site via the indentor and cause the reduction of the indentation force measured by MTM. Therefore, the calculation of stiffness was also reduced.

In summary, it was suggested that the algorithms were feasible for the estimation of mechanical properties of biological soft tissues. The errors and variations might be reduced if more specimens could be tested in future study. Moreover, smaller indentor could be used to reduce the substrate effects so that the effects of misalignment and variations in thickness measurement would be less significant.

Chapter 6 Discussion and Conclusions

The aim of this study was to propose several novel algorithms for estimating the Poisson's ratio and Young's modulus of soft tissue by single-indentation. By the FE study, phantom study and trial application on articular cartilage of bovine patella as introduced in previous chapters, the proposed algorithms were theoretically derived, experimentally validated and their feasibilities were demonstrated. In this chapter, sources of errors, different results of the mechanical properties of soft tissues measured by proposed calculation algorithms, further improvement and applications are discussed as a summary of the results for previous chapters.

6.1 Sources of Errors

In previous chapters (FE study, phantom study and ArtC study), the mechanical properties of various soft tissues were obtained by the indentation algorithms proposed in this study. Differences in the results from different results were observed. One of the reasons for these differences might come from experimental errors. FE simulation could help to conduct a preliminary study and neglect the experimental errors, especially for the errors come from the different settings, environmental factors, displacement, alignment of indentors and so on. In this section, different experimental errors, including the effects of tissue thickness, misalignment of indentor and variation of specimens, were discussed and the subtract effects were also addressed. Moreover, the corresponding improving measures for those errors were

also suggested.

6.1.1 Effects of the Inaccurate Tissue Thickness Measurement

Waters first considered the effects of tissue thickness in the calculation of mechanical properties of soft tissues in 1965 (Waters 1965). In 1972, Hayes and his colleagues also included the parameter of tissue thickness in the calculation algorithm for infinitesimal indentation (Hayes *et al.*, 1972). In equation (3), the tissue thickness was involved in the determination of aspect ratio. Moreover, Zheng and his colleagues further enhanced the infinitesimal indentation with finite deformation effects in 1997 (Zhang *et al*., 1997).

As the parameter of tissue thickness was involved in the calculation of mechanical properties of soft tissues, the thickness measurement played an important role in the calculation. In FE study, the thickness of the model was assigned accurately. Therefore, the effects of the inaccurate tissue thickness measurement would be neglected. In the phantoms and ArtC experiments, the inaccurate thickness measurement was obviously affected the calculation results.

In experiment, over estimation of tissue thickness caused the increase of Kappa value. In equation (4), it showed that the increase of Kappa value due to over estimation of tissue thickness caused the reduction on the estimated value of Young's modulus. This error was found to be more obvious when the material tended to be

incompressible (i.e. Poisson's ratio is close to 0.5) and the aspect ratio was more than one (i.e. larger substrate).

6.1.2 Misalignment of the Indentor

The effects of misalignment of the indentor had been addressed in a previous study (Zheng *et al.*, 1999). If the indentor was not perpendicular to the surface and the underlying substrate, two effects on the calculation of mechanical properties for soft tissue measurement could be observed, including inaccurate measurement of deformation and the changing of boundary conditions.

In FE study, the interface between indentor and specimen together with the underlying material surface was set to be flat thus the misalignment did not happen. For phantom experiment, the surface of the phantom was relatively flat as the top surface of silicone phantom could be flattened due to gravity and diffusion phenomenon during the fabrication of silicone phantom. Therefore, the misalignment of indentor in the experiment of silicone phantom could be minimized.

For ArtC experiment, both the surface of cartilage and interface between the cartilage and underlying bone were totally rough. Moreover, the surface of cartilage and cartilage-bone interface might not be parallel to each other. Furthermore, the variation of tissue thickness of ArtC was found to be large for different sites of patella.

All these factors could contribute to the misalignment of indentor to the ArtC. In this study, indentor with 3mm radius was applied for the mechanical indentation. Smaller size of indentor might help to reduce the effects of indentor misalignment in estimating the Young's modulus and Poisson's ratio.

6.1.3 Variation of Specimens

For the silicone phantoms and ArtC experiments, variation of specimens might be another source of error. In the phantom study, the same procedure and silicone material were used in fabrication in order to minimize the variation. However, the thickness, size, geometry and uneven distributed chemical composition of liquefied silicone and volume of catalyst could cause experimental errors, resulting different mechanical properties. Therefore, average values were used for comparing different proposed calculation algorithms to minimize the effects of specimen variation among the individuals.

For the experiment on ArtC, the variation of mechanical properties among various specimens was more obvious. The variation of the results was mainly due to the differences in thickness and compression modulus. As the indentor and ArtC surface were not totally perpendicular to each other, the measurement of thickness and deformation was relatively difficult to be obtained accurately. Similar to the silicone

phantom test, more specimens of ArtC could be tested in future to minimize the effects.

6.2 Measurement Results of Soft Tissues

In this study, three calculation algorithms were proposed as follows,

1. Double-indentation using Kappa ratio with different sized indentors with consideration of the effects of the finite deformation;
2. Single-indentation using Kappa ratio with two different deformations;
3. Single-indentation using the information of deformation-dependent indentation stiffness.

Using these three calculation algorithms, the Young's modulus and Poisson's ratio could be estimated. Fine Element Analysis, mechanical experiments on silicone phantoms and on articular cartilage were carried out for validating the effectiveness and feasibility of using captioned calculation algorithms. Ideally, the mechanical properties obtained by different mechanical tests should be nearly the same. However, as revealed in Results Chapter the results obtained in our study varied within certain range as discussed in the following sections.

6.2.1 Different Considerations of Single- and Double-Indentation

Compared with single-indentation, there were two concerns for double-indentation, which may cause obvious differences in results. One of the concerns was the variation of the experimental setup and environment between the first and second indentations. If the specimen was biological tissue and had an irregular shape, the changes of temperature, humidity, indentor alignment, ions flow, fluid flow could cause significant changes in mechanical properties. The experimental errors caused by these environmental factors could be diminished by maintaining the environment as stably as possible or minimizing the duration between two indentations, which, however, should be long enough for tissue recovery as discussed in the following paragraph.

The other concern came from the mechanical properties of biological tissue that was visco-elastic. It has been known that the mechanical properties of the soft tissue depend on time. This is because the fluid permeability of the cell membrane keeps changing until the achievement of dynamic equilibrium. Therefore, different durations between the two indentations may contribute to various results for the first and second indentations. For example, if the tissue was compressed in the first indentation, enough time should be given for undergoing relaxation response before the second

indentation. Otherwise, the tissue was compressed again before it completely recovered to its original condition. In that case, the stiffness measured in the second indentation might be relatively larger compared with the results measured in the first indentation. Therefore, longer duration between the two indentations should be given. Combining two concerns a critical time should be identified between the two indentations. Tissue thickness may be measured to ensure the status of the tissue recovery was adequate when the tissue returned to its original thickness level.

In this study, some novel calculation algorithms were developed in order to obtain the data of Young's modulus and Poisson's ratio in single-indentation to provide an alternative measurement due to those drawbacks of double-indentation.

6.2.2 Substrate Effects

In this study, the mechanical properties of biological tissues obtained by indentation were found to be greatly affected by the tissue thickness. It could be assumed that the mechanical properties of underlying materials were significantly stiffer than those of the specimen, such as the metallic platform for silicone phantom and underlying bone under ArtC or skin. Therefore, the Young's modulus measured from biological tissues kept increasing with the decrease of tissue thickness, which was due to substrate effects. The higher stiffness of the substrate might have

contributed to the overall mechanical properties of the specimens.

In 1972, Hayes and his colleagues considered the substrate effect in the single phase indentation model by including the Kappa factor, which was affected by the thickness of specimen and its Poisson's ratio (Hayes *et al.*, 1972). If the specimen was uncompressible, the substrate effect was reflected more obviously on those results.

6.3 Relationships between Deformation and Poisson's Ratio

In the last section, the effects of substrate were discussed. It could not only be used for explaining the difference in measured mechanical properties by using two different sized indentors, but also contributed to the relationships between deformation and Poisson's Ratio. Traditionally, Poisson's ratio was assumed in the calculation in single-indentation. If the indentation was performed on biological tissues simultaneously, the tissue could be considered uncompressible due to the filling of tissue fluid. By the previous study by Zhang *et al.* (1997), it was found that the non-linearity of Poisson's ratio of the single phase model mainly came from the substrate effects. It is because the indentor was being applied to the specimen, the tissue was undergoing deformation based on the applied indentation force. Compressibility of the biological tissue varied due to the different indentation rate, the reaction force from the indented tissue was recorded by the load cell of indentor. As a

circular plane-ended indentor was used, the reaction force contributed by the substrate effects should be non-linear. Therefore, we could estimate the Poisson's ratio via analysis the non-linearity part of the equation.

6.4 Improvement and Further Study

Based on the different sources of errors, some improvements could be carried out in future. So the accuracy for estimation of the mechanical properties of biological tissues could be further enhanced. Further studies on the proposed algorithms were suggested as follows:

i For the kappa factor and beta factor, a more advanced model should be developed. It is because those kappa and beta factors would affect the accuracy of the calculation. As the development of FEA keeps improving, the estimation for those kappa and beta factors may be improved.

ii In this study, linear regression was used to establish the beta table, which was further employed for the estimating Young's modulus and Poisson's ratio. The nonlinear property of the Poisson's ratio was considered to be reflected in the nonlinearity in deformation. In future study, non-linear analysis can be considered to study the relationship between deformation

and the Poisson's ratio, especially for the highly compressible specimen.

iii In future study, indentors with different radii can be prepared for the indentation of specimens with different thickness. In this study, the kappa factor with corresponding aspect ratio was calculated by liner interpolation. However, if the indentor with a specific radius could be used, the error from the interpolation of aspect ratio in the calculation may be reduced.

iv In the present study, the thickness of ArtC was measured by needle punching technique, which would cause irreversible damage to the specimen. Non-destructive measures can be applied in the future study for thickness measurement such as optical or ultrasonic methods. All these methods can be applied in different kinds of biological tissues for *in-vivo* testing.

v In the trypsin digestion of ArtC, a study on the effects of trypsin digestion on the change of tissue thickness should be carried out in future. As the trypsin digests the PGs content in ArtC, the thickness may be changed, which would affect the results of estimation of mechanical properties.

vi With the development of ultrasound technology, the indentation may not be necessary to be carried out by material testing machine. Hand-held device, such as Tissue Ultrasound Palpation System (TUPS) can be used with the

proposed algorithms to carry out *in-vivo* measurement on different kinds of biological tissues.

vii In this study, linear elastic model was applied. Other models may be used in future, such as non-linear visco-elastic model. So the biomechanical properties of the solid phase of biological tissue can also be obtained separately. Moreover, the relationships between indentation rate and measurement of the Poisson's ratio should be further explored.

viii In future studies, different kinds of biological soft tissues can be tested by the proposed algorithms to further test their performances and obverse different tissue's responses to the proposed algorithms.

6.5 Conclusions

In this study, several calculation algorithms were proposed for the estimation of Poisson's ratio and Young's modulus of soft tissue by single indentation. By FE study and practical experiments on both silicone phantom and ArtC, the feasibility of applying the proposed calculation algorithms for determining soft tissue mechanical properties was demonstrated. Through this study, following conclusions were drawn:

i The effect of finite deformation on the estimation of Young's modulus should be more significant compared to that effect on the calculation of Poisson's ratio. The

finite deformation effects would be more significant if the compressibility of the tissue tends to be lower.

ii Kappa factor for compensating the finite deformation effects might help to improve the accuracy of the estimation of Young's modulus together with Poisson's ratio of soft tissue by indentation.

iii For the proposed algorithm for estimating Young's modulus and Poisson's ratio using single-indentation with t different deformations, the performance could be greatly improved if the aspect ratio of the specimen under test was or greater than 1.0. For the *in-vivo* measurement, this method should be more suitable for the thinner soft tissue.

iv In phantom study, two different silicone phantoms were used. The feasibility of using the proposed algorithms for estimating Young's modulus and Poisson's ratio was demonstrated. The percentage error of the estimated Poisson's ratio was found to be less than 10%.

v In phantom study, the percentage error of the estimated Young's modulus in the softer silicone phantom was found to be more obvious. It might be caused by the experimental errors such as the misalignment of indentor, the unsmooth surface of specimen and errors in thickness measurement.

vi In ArtC experiment, Young's modulus and Poisson's ratio of the ArtC were

obtained by single-indentation with the deformation-dependent indentation stiffness and single-indentation with the information of different deformations. The percentage change of the results obtained by the two methods was less than 10 %.

vii In ArtC experiment, the percentage changes of the Young’s modulus measured before and after trypsin digestion were ranged from -45% to -71%. It was demonstrated that the proposed algorithms would be used to determine the changes of the mechanical properties of soft tissues.

Reference

Athanasiou, K. A., Rosenwasser, M. P., Buckwalter, J. A., Malinin, T. I. and Mow, V. C., Interspecies comparisons of in situ intrinsic mechanical properties of distal femoral cartilage. J. Orthop. Res., 9, 330-340, 1991.

Armstrong, C. G. and Mow, V. C., Variations in the intrinsic mechanical properties of human articular cartilage with age, degeneration and water content. J. Bone Joint Surg. 64A, 88, 1982.

Arokoski, J., Jurvelin, J., Kiviranta, I., Tammi, M. and Helminen, H. J., Softening of the lateral condyle articular cartilage in the cannie knee joint after long distance (up to 40km/day) running training lasting one year. J. Sports Med., 15, 254-260, 1994.

Bauer, M., Mazza, E., Nava, A., Zeck, W., Eder, M., Bajka, M., Cacho, F., Lang, U. and Holzapfel, G. A., In vivo Characterization of the mechanics of human uterine cervice., Ann. N. Y. Acad. Sci., 1101, 186-202, 2007.

Buckwalter, J. A. and Mankin, H. J., Articular cartilage, part II: degeneration and osteoarthritis, repair, regeneration, and transplantation. J. Bone Joint Surg. Am., 79(4), 612-632, 1997.

Buckwalter, J. A. and Mankin, H. J., Articular cartilage: degeneration and osteoarthritis, repair, regeneration and transplantation. In: Cannon, J. D., Eds., Instructional Course Lectures 47. American Academy of Orthopaedic Surgeons, 1998, 487-504.

Bullough, P. G. and Jagannath, A., The morphology of the calcification front in articular cartilage. Its significance in joint function, J. Bone Joint Surg. [Br.], 65, 72-78, 1983.

Chahine, N. O., Wang, C. C. B., Hung, C. T. and Ateshian, G. A., Ansiotropic strain-dependent material properties of bovine articular cartilage in the transitional range from tension to compression. J. Biomech., 37, 1251-1261, 2004.

Choi, A. P. C. and Zheng, Y. P., Estimation of Young's modulus and Poisson's ratio of soft tissue from indentation using two different-sized indentors: finite element analysis of the finite deformation effect. Med. Biol. Eng. Comp., 43, 258-264, 2005.

Dawes-Higgs, E. K., Swain, M. V., Higgs, R. J. E. D., Appleyard, R. C. and Kossard, S., Accuracy and reliability of a dynamic biomechanical skin measurement probe for the analysis of stiffness and viscoelasticity. Phys. Measurement, 25(1), 97-105, 2004.

DiSilvestro, M. R. and Suh, K. J. K., A cross-validation of the biphasic poroviscoelastic model of articular cartilage in unconfined compression, indentation, and confirmed compression. J. Biomech., 34(4), 519-525, 2001.

Dokos, S., LeGrice, I. J., Smaill, B. H., Kar, J. and Young, A. A., A triaxial-measurement shear-test device for soft biological tissues. J. Biomech. Eng., 122, 471-478, 2000.

Fleming, B. C. and Beynnon B. D., In Vivo Measurement of Ligament/ Tendon Strains and Forces: A Review. Ann. Biomed. Eng., 32, 318-328, 2004.

Fung, Y. C., Stress – strain history relations of soft tissues in simple elongation. In: Biomechanics: Its Foundations and Objectives, Fung, Y. C., Perrone, N. and Anliker, M., eds., Englewood Cliffs, NJ: Prentice Hal, Inc., 181-207, 1972.

Fung, Y. C., Bio-viscoelastic solids, In: Biomechanics: Mechanical Properties of Living Tissues, New York: Springer-Verlag, 196-260, 1981.

Garn, S. M., Comparison of pinch caliper and x-ray measurements of skin plus subcutaneous fat. Science., 124, 178-179, 1956.

Gefen, A., Megido-Ravid, M., Azariah, M., Itzchak, Y. and Arcan, M., Integration of plantar soft tissue stiffness measurements in routine MRI of the diabetic foot. Clin. Biomech., 16, 921-925, 2001.

Goss, S. A., Johnston, R. L. and Dunn, F., Compilation of empirical ultrasonic properties of mammalian-tissues, J. Acoust. Soc. Am., 68, 93-108, 1980.

Grant, W. P., Foreman, E. J., Wilson, A. S., Jacobus, D. A. and Kukla, R. M., Evaluation of Young's modulus in Achilles Tendons with Diabetic Neuroarthropathy. J. Am. Podiatr. Med. Assoc., 95(3), 242-246, 2005.

Han, L., Noble, J. A. and Burcher, M., A novel ultrasound indentation system for measuring biomechanical properties of in-vivo soft tissue. Ultrasound in Med. & Biol., 29, 813-823, 2003.

Hasler, E. M., Herzog, W., Wu, J. Z., Muller, W and Wyss, U., Articular cartilage biomechanics: Theoretical models, material properties, and biosynthetic response. Critical Reviews in Biomed Eng., 27(6), 415-488, 1999.

Hayes, W. C. and Mockros, L. F., Viscoelastic properties of human articular cartilage. J. Appl. Physiol., 31(4), 562-568, 1971.

Hayes, W. C., Keer, L. M., Herrman, G. and Mockros, L. F., A mathematical analysis for indentation tests of articular cartilage. J. Biomech., 5, 541-551, 1972.

Hoch, D. H., Grodzinsky, A. J., Koob, T. J., Alevert, M. L. and Eyre D. R., Early changes in material properties of rabbit articular cartilage after meniscectomy, J. Orthop. Res., 1, 4-12, 1983.

Hollenstein M., Mechanical characterization of soft materials: Comparison between different experiments on synthetic specimens. Diploma Thesis, Centre of Mechanics, ETH Zurich.

Hollenstein, M., Nava, A., Valtorta, D., Snedeker, J. G. and Mazza E., Mechanical characterization of the liver capsule and parenchyma. Proc. Lecture Notes in Comput. Science, 4072: 150-158, 2006.

Horikawa, M., Ebihara, S., Sakai, F. and Akiyama, M., Noninvasive measurement method for hardness in muscular tissues, Med. Biol. Eng. Comput., 31(6), 623-627, 1993.

Huang, C. Y., Mow, V. C. and Ateshian, G. A., The role of flow-independent viscoelasticity in the biphasic tensile and compressive responses of articular cartilage, J. Biomech. Eng. 123(5), 410-417, 2001.

Hunag, Y. P., Zheng, Y. P. and Leung, S. F., Quasi-linear viscoelastic properties of fibrotic neck tissues obtained from ultrasound indentation tests in vivo, Clin. Biomech. 20, 145-154, 2005.

Huang, Y. P., Zheng, Y. P., Leung, S. F. and Mak, A. F. T., Reliability of measurement of skin ultrasonic properties in vivo: a potential technique for assessing irradiated skin, Skin Res. Tech. 13(1), 55-61, 2007a.

Huang Y. P., Zheng, Y. P., Leung, S. F. and Choi, A. P., High frequency ultrasound assessment of skin fibrosis: clinical results, Ultrasound in Med. & Biol. 33(8), 1191-1198, 2007b.

Jacquemoud, C., Bruyere-Garnier, K. and Coret, M., Methodology to determine failure characteristics of plantar soft tissues using a dynamic tensile test, J. Biomech., 40, 468-475, 2007.

Jin, H. and Lewis, J. L., Determination of Poisson's ratio of articular cartilage by indentation using different sized indenters. J. Biomech. Eng., 126, 138-145, 2004.

Jurvelin, J., Kiviranta, I., Arokoski, J., Tammi, M. and Helminen, H. J., Indentation study of the biomechanical properties of articular cartilage in the canine knee, Eng. Med., 16, 15-22, 1987.

Jurvelin, J., Saamanen, A. M., Arokoski, J., Helminen, H. J., Kiviranta, I. and Tammi, M., Biomechanical properties of the canine knee articular cartilage as related to matrix proteoglycans and collagen. Eng. Med., 17, 157-162, 1988.

Jurvelin, J., Kiviranta, I., Saamanen, A. M., Tammi, M. and Helminen, H. J., Indentation stiffness of young cannie knee articular cartilage: Influence of strenuous joint loading. J. Biomech., 23, 1239-1246, 1990.

Jurvelin, J., Biomechanical properties of the knee articular cartilage various loading conditions. Ph. D. Dissertation, Kuopio University of Kuopio, 1991.

Jurvelin, J., Rasanen, T, Kolmonen, P. and Lyyra, T., Comparison of optical, needle probe, and ultrasonic techniques for the measurement of articular cartilage thickness, J. Biomech., 28, 231-235, 1995.

Jurvelin, J. S., Buschmann, M. D. and Hunziker, E. B., Optical and mechanical determination of Poisson's ratio of adult bovine humeral articular cartilage, J. Biomech., 30(3), 235-241, 1997.

Jurvelin, J. S., Arokoski, J. P. A., Hunziker, E. B. and Helminen, H. J., Topographical variation of the elastic properties of articular cartilage in the canine knee. J. Biomech., 33, 669-675, 2000.

Kempson, G. E., Freeman, M. A. R. and Swanson, S. A. V., The determination of a creep modulus for articular cartilage from indentation tests on the human femoral head. J. Biomech., 4, 239-250, 1971.

Khatyr, F., Imberdis, C., Vescovo, P., Varchon, D. and Lagarde, J. M., Model of the viscoelastic behaviour of skin in vivo and study of anisotropy. Skin Res. Tech., 10(2), 96-103, 2004.

Klaesner, J. W., Commean, P. K., Hastings, M. K., Zou, D. and Mueller, M. J., Accuracy and reliability testing of a portable soft tissue indentor. IEEE Trans. Neural Syst. Rehabil. Eng., 9, 232-240, 2001.

Klaesner, J. W., Hastings, M. K., Zou, D., Lewis, C. and Mueller, M. J., Planter tissue stiffness in patients with diabetes mellitus and peripheral neuropathy. Arch. Phys. Med. Rehabil., 83, 1796-1801, 2002.

Kristy, B., Arbogast, K. L., Thibault, B., Scott, P., Karen, I. W. and Susan S. M., A high-frequency shear device for testing soft biological tissues. J. Biomech., 30(7), 757-759, 1997.

Lafrance, H., Guillot, M., Germain, L. and Auger, F. A., A method for the evaluation of tensile properties of skin equivalents. Med. Eng. Phy., 17(7), 537-543, 1995.

Lai, W. M., Mow, V. C. and Roth, V., Effects of a nonlinear strain-dependent permeability and rate of compression on the stress behaviour of articular cartilage. J. Biomech. Eng., 103, 221-231, 1981.

Lai, W. M., Hou, J. S. and Mow, V. C., A triphasic theory for the swelling and deformation behaviors of articular cartilage. J. Biomech. Eng., 113(3), 245-258, 1991.

Lau, J. C. M., Li-Tsang, C. W. P. and Zheng, Y. P., Application of tissue ultrasound palpation system (TUPS) in objective scar evaluation. Burns, 31, 445-452, 2005.

Leung, S. F., Zheng, Y. P., Choi, C. Y. K., Mak, S. S. S., Chiu, S. K. W., Zee, B. and Mak, A. F. T., Quantitative measurement of post-irradiation neck fibrosis based on Young's modulus: description of a new method and clinical results. Cancer. 95, 656-662, 2002.

Lin, R. M., Chang, G. L. and Chang, L. T., Biomechanical properties of muscle-tendon unit under high-speed passive stretch. Clin. Biomech., 14(6), 412-417, 1999.

Linder-Ganz, E. and Gefen, A., Mechanical compression-induced pressure sores in rat hindlimb: muscle stiffness, histology, and computational models. J. Appl. Phys. 96(6), 2034-2049, 2004.

Lu, M. H., Zheng, Y. P. and Huang, Q. H., A Novel noncontact ultrasound indentation system for measurement of tissue material properties using water jet compression. Ultrasound in Med. & Biol., 31(6), 817-826, 2005.

Mak, A. F., Apparent viscoelastic behavior of articular cartilage – contributions from intrinsic matrix viscoelasticity and interstitial fluid flow. J. Biomech. Eng., 108, 123-130, 1986.

Mak, A. F., Lai, W. M. and Mow, V. C., Biphasic indentation of articular cartilage – I. Theoretical analysis. J. Biomech., 7, 703-714, 1987.

Mak, A. F. T., Liu, G. H. W. and Lee, S. Y., Biomechanical assessment of below – knee residual limb tissue. J. Rehabil. Res. Develop., 31(3), 188-198, 1994.

Mankin, H. J., Mow, V. C. and Buckwalter, J. A., Articular cartilage repair and osteoarthritis. In: Buckwalter, J. A., Einhorn, T. A. and Simon, S. R., Eds., Orthopaedic Basic Science: Biology and Biomechanics of the Musculoskeletal System, 2nd ed., American Academy of Orthopaedic Surgeons, 2000, 443-488.

Mansour, J. M., Biomechanics of Cartilage. In: Oatis, C. A., Eds., Kinesiology: The Mechanics & Pathomechanics of Human Movement, 1st ed., Philadelphia, Lippincott Williams & Wilkins, 2004, 66-79.

Mazza, E., Nava, A., Hahnloser, D., Jochum, W. and Bajka, M., The mechanical response of human liver and its relation to histology: An *in vivo* study, Med. Image Anal., 11, 663-672, 2007.

Moody, H. R., Brown, C. P., Bowden, J. C., Crawford, R. W., McElwain, D. L. S. and Oloyede, A. O., *In-vitro* degradation of articular cartilage; dose trypsin treatment produce consistent results. J. Anat., 209, 259-267, 2006.

Mow, V. C., Lai, W. M. and Redler, I., Some surface characteristics of articular-cartilage. A scanning electron miscopy study and a theoretical model for the dynamic interaction of synovial fluid and articular cartilage. J. Biomech., 7, 449, 1974.

Mow, V. C., Kuei, S. C., Lai, W. M. and Armstrong, C. G., Biphasic creep and stress-relaxation of articular cartilage in compression. J. Biomech. Eng., 102(1), 73-84, 1980.

Mow, V. C., Gibbs, M. C., Law, W. M., Zhu, W. B. and Athanasiou, K. A., Biphasic indentation of articular cartilage – II. A numerical algorithm and experimental study. J. Biomech., 22, 853-861, 1989.

Mow, V. C. and Ratcliffe, A., Structure and function of articular cartilage and meniscus. In: Mow, V. C. and Hayes, W. C., Eds., Basic Orthopaedic Biomechanics, Philadelphia, Lippincott-Raven, 1997, 113-177.

Mow, V. C. and Hung, C. T., Biomechanics of articular cartilage. In: Nordin, M. and Frankel, V. H., Eds., Basic Biomechanics of the Musculoskeletal System, 3rd ed., Philadelphia, Lippincott Williams & Wilkins, 2001, 60-100.

Mow, V. C., Gu, W. Y. and Chen, F. H., Structure and function of articular cartilage and meniscus. In: Mow, V. C. and Huiskes, R., Eds., Basic Orthopaedic Biomechanics And Mechano-Biology, 3rd ed., Philadelphia, Lippincott Williams & Wilkins, 2005, 181-258.

Nava, A., Mazza, E., Kleinermann, F., Avis, N. J. And McClure, J., Determination of the mechanical properties of soft tissues through aspiration experiments. Med. Image Comput. Comput. Assist. Interv. MICCAI 2003, 2878: 222-229, 2003.

Nieminen, M. T., Toyras, J., Laasanen, M. S., Silvennoinen, J., Heliminen, H. J. and Jurvelin, J. S., Prediction of biomechanical properties of articular cartilage with quantitative magnetic resonance imaging. J. Biomech., 37, 321-328-2004.

Newton, P. M., Mow, V. C., Gardner, T. R., Buckwalter, J. A. and Albrigth, J. P., The effect of liftlong exercise on cannie articular cartilage, Am. J. Sports Med., 25, 282-287, 1997.

Nordin, M., Lorenz, T. and Campello, M., Biomechanics of tendons and ligaments. In: Nordin, M. and Frankel, V. H., Eds., Basic biomechanics of the musculoskeletal system, Philadelphia, Lippincott Williams & Wilkins, 2001, 102-126.

Oilarinen, A. and Knuutinen, A., Mechanical Properties of Human Skin: Biochemical Aspects. In: Elsner, P., Berardesca, E., Wilhelm, K., P. and Maibach, H. I., Eds., Bioengineering of the skin: Skin Biomechanics, New York, CRC Press, 2002, 3-16.

Parsons, J. R. and Black, J., The viscoelastic shear behavior of normal rabbit articular cartilage. J. Biomech., 10, 21-29, 1977.

Pedersen, L., Hansen, B. and Jemec, G. B. E., Mechanical properties of the skin: A comparison between two suction cup methods. Skin Res. Technol. 9:111-115, 2003.

Patil, S. G. and Zheng, Y. P., Measurement of ultrasound speed of articular cartilage in variable conditions. Conf Proc IEEE Eng. Med. Biol. Soc., 2, 1341-1344, 2004.

Rasanen, T. and Messner, K., Regional variations of indentation stiffness and thickness of normal rabbit knee articular cartilage. J. Biomed. Mat. Res., 31, 519-524, 1996.

Roth, V. and Mow, V. C., The intrinsic tensile behavior of the matrix of bovine articular cartilage and its variation with age. J Bone Joint Surg., 62A, 1102, 1980.

Schinagl, R. M., Gurskis, D., Chen, A. C. and Sah, R. L., Depth-dependent confined compression modulus of full-thickness bovine articular cartilage. J. Ortho. Res., 15(4), 499-506, 1997.

Setton, L. A., Mow, V. C., Mueller, F. J., Pita, J. C. and Howell, D. S., Mechanical properties of canine articular cartilage are significantly altered following transaction of the anterior cruciate ligament. J. Orthop. Res., 12, 451-463, 1994.

Spilker, R. L., Suh, J. K. and Mow, V. C., A finite element analysis of the indentation stress-relaxation response of linear biphasic articular cartilage. J. Biomech. Eng., 114, 191-201, 1992.

Suh, J. K. F., Youn, I. and Fu, F. H., An in situ calibration of an ultrasound transducer: a potential application for an ultrasonic indentation test of articular cartilage. J. Biomech., 34, 1347-1353, 2001.

Swann, A. C. and Seedhom, B. B., Improved techniques for measuring the indentation and thickness of articular cartilage. Proc. Inst. Mech. Eng [H]., 203(3), 143-150, 1989.

Tobias, L. and Campello, M. adapted from Pitman, M. I. and Lars-Peterson, L., Biomechanics of skeletal muscles. In: Nordin, M. and Frankel, V. H., Eds., Basic biomechanics of the musculoskeletal system, Philadelphia, Lippincott Williams & Wilkins, 2001, 148-176.

Toyras, J., Lyyra-Laitinen, T., Niinimaki, M., Lindgren, R., Nieminen, M. T., Kiviranta, I. and Jurvelin, J. S., Estimation of the young's modulus of articular cartilage using an arthoscopic indentation instrument and ultrasonic measurement of tissue thickness. J. Biomech., 34, 251-256, 2001.

Uitto, J., Olsen, D. R. and Fazio, M. J., Extracellular Matrix of the skin: 50 Years of progress. J. Invest. Dermatol. 92, S61-S77, 1989.

Vannah, W. M., Drvaric, D. M., Hastings, J. A. and Harning, D. M., A method of residual limb stiffness distribution measurement. J. Rehabil. Res. Develop., 36, 1-7, 1999.

Wang, C. C. B., Hung, C. T. and Mow, V. C., An analysis of the effects of depth-dependent aggregate modulus on articular cartilage stress – relaxation behavior in compression. J. Biomech., 34, 75-84, 2001.

Wang, C. C. B., Chahine, N. O., Hung, C. T. and Ateshian, G. A., Optical determination of anisotropic material properties of bovine articular cartilage in compression. J. Biomech., 36, 339-353, 2003.

Wang, J., Brienza, D. M., Yuen, Y. W., Karg, P. and Xue, Q., A compound sensor for biomechanical analysis of buttock soft tissue in vivo, J. Rehabil. Res. Develop., 37(4), 433-443, 2000.

Waters, N. E., The indentation of thin rubber sheets by spherical indentors. Brit. J. Appl. Phys., 16, 557-563, 1965.

Waters, N. E., The indentation of thin rubber sheets by cylindrical indentors. Brit. J. Appl. Phys., 16, 1387-1392, 1965.

Wu, J. Z., Dong, R. G., Smutz, W. P. and Schopper, A. W., Nonlinear and viscoelastic characteristics of skin under compression: experiment and analysis. Bio. Med. Mat. Eng., 13(4), 373-385, 2003.

Wu, J. Z., Cutlip, R. G., Andrew, M. E. and Dong, R. G., Simultaneous determination of the nonlinear-elastic properties of skin and subcutaneous tissue in unconfined compression tests. Skin Res. Tech., 13(1), 34-42, 2007.

Zhang, M., Zheng, Y. P. and Mak, A. F. T., Estimating the effective Young's modulus of soft tissues from indentation tests – nonlinear finite element analysis of effects of friction and large deformation. Med. Eng. Phys., 19, 512-517, 1997.

Zheng, Y. P. and Mak, A. F. T., An ultrasound indentation system for biomechanical properties assessment of soft tissue in-vivo. IEEE Trans. Biomed. Eng., 43, 912-918, 1996.

Zheng, Y. P. and Mak, A. F. T., Effective elastic properties for lower limb soft tissues from manual indentation experiment. IEEE Trans. Rehabil. Eng., 7, 257-267, 1999a.

Zheng, Y. P. and Mak, A. F. Y., Extraction of quasi linear viscoelastic parameters for lower limb soft tissues from manual indentation experiment. J. Biomech. Eng., 121, 330-339, 1999b.

Zheng, Y. P., Mak, A. F. T. and Lue, B. K., Objective assessment of limb tissue elasticity: Development of a manual indentation procedure. J. Rehabil. Res. Develop., 36, 71-85, 1999.

Zheng, Y. P., Choi, Y. K. C., Wong, K., Chan, S. and Mak, A. F. T., Biomechanical assessment of plantar foot tissue in diabetic patients using an ultrasound indentation system. Ultrasound in Med. & Biol., 26, 451-456, 2000.

Zheng, Y. P., Patil, S. and Wang, Q., Ultrasound speed in articular cartilage under different bathing saline concentration. Advanced Nondestructive evaluation I, PTS 1 and 2, Proceeding key engineering materials, 321-323, 972-977, 2006.